Electron scattering from ^{10}B

A. Cichocki, J. Dubach, R. S. Hicks, and G. A. Peterson
Department of Physics and Astronomy, University of Massachusetts, Amherst, Massachusetts 01003

C. W. de Jager, H. de Vries, and N. Kalantar-Nayestanaki*
National Institute for Nuclear Physics and High-Energy Physics, Section K, Amsterdam, The Netherlands

T. Sato
Department of Physics, Osaka University, Toyonaka, Osaka 560, Japan
(Received 11 January 1995)

Electron scattering measurements have been made in order to determine the longitudinal and transverse form factors of low-lying levels in ^{10}B. With the exception of the broad 5.18 MeV level, results were obtained for all known levels up to 6.7 MeV. The measurements span the momentum transfer range q =0.48–2.58 fm^{-1}. The primary objective of this work was to improve the data on the pure isovector $M3$ form factor of the 1.740 MeV excitation, the transform of which yields the $1p_{3/2}$ single-nucleon wave function. A Woods-Saxon potential was found to provide a much better representation of the data than the harmonic oscillator model, and the rms size of this orbit was determined to be 2.79 ± 0.11 fm in the relative core-particle coordinate frame. Nevertheless, confidence in the quantitative details of this interpretation is hindered by conflicting evidence regarding the contribution of core polarization. Our analysis of the Coulomb elastic form factor gave an rms radius for the ground-state charge distribution equal to $2.58 \pm 0.05 \pm 0.05$ fm, slightly larger than values previously published. Longitudinal and transverse form factors deduced for inelastic transitions were compared with theoretical results of conventional $1p$-shell models, models with $1\hbar\omega$ and $2\hbar\omega$ configurations involving the $1s$, $2s1d$, and $2p1f$ shells, and finally, a model that included core polarization. Although restricted $1p$-shell models were found to provide good predictions for the ^{10}B natural-parity level spectrum and transverse form factors, they were less successful for $C2$ form factors: not only is there a considerable dependence on the $1p$-shell interaction, but these models give just 45% of the total observed $C2$ transition strength. Only a 10% improvement was realized by expanding the shell model space to include $2\hbar\omega$ configurations. The inclusion of even higher-excited configurations by means of core polarization calculations was essential to remove the remaining shortfall.

PACS number(s): 25.30.Bf, 25.30.Dh, 27.20.+n

I. INTRODUCTION

In this paper are presented the first comprehensive, high-resolution measurements of the electron-scattering form factors of ^{10}B. The primary motivation for these measurements derives from the distinctive pure isovector $M3$ excitation to the J^π=0$^+$, T=1 state at 1.740 MeV which, in $1p$-shell models, arises from a "stretched" spin-flip transition of a $1p_{3/2}$ nucleon. Thus the (e,e') form factor is given solely in terms of the $1p_{3/2}$ wave function

$$F_{M3}(q) \propto q\mu_1 \int_0^\infty | R_{p_{3/2}}(r) |^2 j_2(qr) r^2 dr \ , \qquad (1)$$

where q is the electron-scattering momentum transfer, r is the nuclear radial coordinate, and the isovector magnetic moment is given by the difference between the proton and neutron magnetic moments: $\mu_1=(\mu_\pi - \mu_\nu)/2$. Equation (1) can be transformed to yield the single-particle radial wave function $R_{p_{3/2}}(r)$ within the nuclear interior, not merely the rms orbital size as has been the case with previous magnetic (e,e') results [1].

The $1p_{3/2}$ wave function deduced from our earlier measurements of this $M3$ form factor at the MIT-Bates accelerator [2] has been used in the interpretation of ^{10}B(p,p'), ^{10}B(p,n), and ^{10}B$(\vec{p},\vec{p}')$ measurements [3–5]. In the latter case [5], for example, this constraint led to the inference that the ratio of transverse to longitudinal spin couplings in the effective NN interaction was larger than for free NN scattering. The availability of the wave function also provides a unique opportunity to test the understanding of single-nucleon knockout processes, in particular the $(e,e'p)$ reaction which in recent years has emerged as the most general and powerful method for studying the single-nucleon properties of nuclei. According to the quasifree knockout picture, cross sections measured in $(e,e'p)$ experiments are directly proportional to the square of the wave function of the ejected proton. In principle, then, the $1p_{3/2}$ wave function could also be obtained from measurements of the ^{10}B$_{J^\pi=3^+}(e,e'p)^9$Be$_{3/2^-}$ reaction. However, the interpre-

*Permanent address: Kernfysisch Versneller Instituut, Groningen, The Netherlands.

tation of $(e,e'p)$ results is compromised by uncertainties in the description of effects such as final-state interactions, multistep processes, and meson-exchange currents. In the case of ^{10}B, the information on the single-particle wave function derived from (e,e') provides a valuable constraint for identifying the consequences of these effects.

Before undertaking new high-resolution measurements of the ^{10}B$(e,e'p)$ reaction, it is first necessary to improve the quality of the (e,e') data for the 1.740 MeV $M3$ transition: The $\approx 20\%$ uncertainties of prior measurements [6] at $q < 2$ fm^{-1} limited the information that could be obtained on the wave function at large r, corresponding to small nucleon momentum, the region for which $(e,e'p)$ cross sections are most favorable.

Another important motivation for the present work is derived from recent core-polarization studies [7] which bring into question the extent to which the $M3$ excitation may be simply represented as a spin-flip transition of a $1p_{3/2}$ nucleon. In our previous investigation [2], calculations using conventional $1p$-shell amplitudes and Woods-Saxon wave functions were found to be in excellent quantitative agreement with $M3$ form factors of ^{10}B and ^{11}B. This observation appears to confirm the notion that configurations involving particles or holes outside the $1p$ shell have only a minor influence on $M3$ form factors. Although additional calculations showed that meson-exchange contributions could raise the predicted $M3$ form factors by $\approx 15\%$, the enhancement was almost independent of q and hence the extracted radial wave functions were essentially unaffected. As we have implied, however, the core-polarization studies suggest an alternative interpretation, which will be examined further below.

The scope of this work was not confined to the 1.740 MeV $M3$ excitation: Because of the good experimental resolution and 10% momentum acceptance of the electron spectrometer, data were obtained, with one exception, on all known levels of ^{10}B below 6.7 MeV. Most of these levels had not been observed in earlier (e,e') studies [6,8–12], and where previous results are available, the statistical precision and kinematic range are improved by the new measurements.

The data for elastic scattering were analyzed with the goal of seeking information on the ground-state charge density; inelastic cross sections were found to derive mainly from the longitudinal quadrupole ($C2$) and octupole ($C3$) operators. Particularly for electric quadrupole excitations, it has long been recognized [13] that these transitions have highly collective properties: Radiative decay widths and form factors often exceed shell model predictions by factors of 2 or more. Quantitative explanations of the augmented electric transition strength have consequently relied on collective treatments [14] such as phenomenological hydrodynamic and rotational models, as well as calculations in which lowest-order single-particle configurations are mixed with collective giant resonances. The availability of core-polarization calculations to supplement usual shell-model treatments represents an alternative, more microscopic attempt to describe these longitudinal excitations. More generally, the existence of new (e,e') data on previously unmeasured excitations in ^{10}B allows the core polarization treatment to be tested much more comprehensively than was previously possible.

II. EXPERIMENTAL DETAILS AND DATA ANALYSIS

The experiment was performed using the electron-scattering facility [15] at NIKHEF-K. Self-supporting targets were formed by pressing boron powder, isotopically enriched in ^{10}B. A B_4C mortar and pestle was utilized to first grind the boron powder to pass through a 250 mesh sieve, corresponding to a grain size of approximately 10–50 μm. This powder was then mixed with 1–2 % by mass of polystyrene binder in a chloroform solution and hot pressed at 2.8×10^7 Pa using a tungsten carbide punch and die. While in the press the temperature of the targets reached 140 °C, exceeding the $\approx$ 115 °C softening temperature of polystyrene. The pressed targets, measuring 1.27×3.81 cm^2, were allowed to cool on the die, and then floated free with a few drops of liquid nitrogen. A final heating in air was found to further strengthen the targets.

As a result of evaporation of the chloroform solvent, the composition of the target material was little changed by the addition of the binder solution. A subsequent determination by means of elastic electron scattering at low momentum transfer gave the atomic composition as 97.7% ^{10}B, 2.0% ^{11}B, and 0.3% ^{12}C, close to the values specified by the supplier of the boron [16]. Several targets were pressed. The thickness of those utilized for the measurements was 38.0 and 70.0 mg cm^{-2}.

Despite being self-supporting and relatively pure in ^{10}B, these targets performed with only qualified success because of their fragility to heat deposited by the incident electron beam: Beam currents had to be restricted to < 10 μA in order to avoid destroying the targets. At one point during the experiment the 38.0 mg cm^{-2} thick target broke, resulting in a number of measurements being made on a target of unknown and irregular thickness. These data were subsequently salvaged by means of a normalization procedure that will be discussed later. Isotopically enriched $^{10}B_4C$ would constitute a more robust target that may be preferable for future experimental investigations on boron isotopes.

Scattered electrons were detected in a QDD magnetic spectrometer [15]. The maximum solid angle of this spectrometer is defined by a 80×80 mrad^2 octagonal aperture, corresponding to an acceptance of 5.6 msr. Because of count-rate considerations, measurements were also made using a square-aperture collimator that restricted the spectrometer angular acceptance to 20×20 mrad^2. Spectra were measured up to an excitation energy of about 7 MeV for six different incident electron energies E_0 ranging from 82 to 453 MeV and scattering angles between 30.2° and 140.0°, corresponding to a momentum transfer range of 0.48–2.58 fm^{-1}. Cross sections were extracted by line-shape fitting the measured spectra and applying corrections for radiative and ionization ef-

fects. Details of the analysis procedures have been given elsewhere [17]. An example of a measured spectrum and resultant fit is shown in Fig. 1. In addition to the 1.74 MeV peak, extensive data were acquired on 11 other excitations, many of which were resolved for the first time in an electron-scattering experiment. The full-width-at-half-maximum energy resolution of the experiment varied with kinematic conditions and target thickness, ranging from 26 to 115 keV.

For each ^{10}B spectrum, cross-section measurements were also made of elastic scattering from ^{12}C. These data were compared to the results of distorted-wave Born approximation (DWBA) calculations based on the charge density of ^{12}C, which is well known [18]. The deduced normalization factors were then utilized to fix the absolute scale of all ^{10}B data taken on sound targets. Finally, we relied upon the correctly normalized results for elastic scattering from ^{10}B to establish the normalization of inelastic data acquired with broken targets: The good ^{10}B elastic results were combined with data from a previous experiment [12] and fitted in the DWBA with an incoherent sum of $C0$ and $C2$ form factors as described in Sec. IV A 1. The associated $C0$ and $C2$ densities were then utilized for DWBA calculations of reference elastic cross sections at the kinematics of data taken with broken targets.

In the plane-wave Born approximation, the cross section for electron scattering can be written [19] in terms of longitudinal and transverse form factors F_L and F_T:

$$\frac{d\sigma}{d\Omega} = \frac{d\sigma_M}{d\Omega}\eta\left[F_L^2(q) + \left(\frac{1}{2} + \tan^2\frac{\theta}{2}\right)F_T^2(q)\right] , \quad (2)$$

where

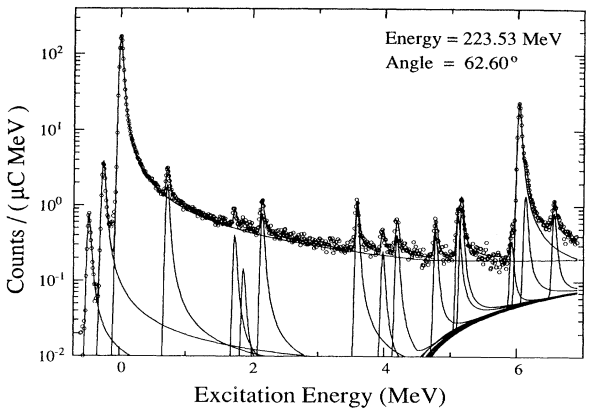

FIG. 1. Example of a measured ^{10}B(e,e') spectrum. Some of the peaks are due to contaminants in the target; e.g., the two leftmost peaks correspond to elastic scattering from ^{12}C and ^{11}B. The curves are the result of a peak-fitting procedure used to determine cross sections for individual excitations. The monotonically increasing background at the right of the spectrum was introduced to account for continuum breakup. For this spectrum the full-width-at-half-maximum energy resolution was 30 keV.

$$\eta = \left(1 + 2E_0\sin^2\frac{\theta}{2}/M_t\right)^{-1}$$

corrects for nuclear recoil. In these equations E_0 represents the incident electron energy, θ is the scattering angle in the laboratory, and M_t is the mass of the target nucleus. The Mott cross section

$$\frac{d\sigma_M}{d\Omega} = \frac{Z^2\alpha^2\cos^2\frac{\theta}{2}}{4E_0^2\sin^4\frac{\theta}{2}}$$

is for scattering from point charge Ze, $\alpha \approx 1/137$ is the fine-structure constant, and

$$q^2 \approx 4E_0^2\eta\sin^2\frac{\theta}{2}$$

is the square of the three-momentum transfer.

According to the Rosenbluth procedure, the longitudinal and transverse form factors can be separated by making measurements at the same q but different values of $(1/2+\tan^2\theta/2)$, the virtual photon polarization factor in Eq. (2). To a large extent the kinematics of the present experiment satisfy this requirement, although some interpolation in momentum transfer is required. In order to do this, the data were first separated according to the value of polarization factor to provide initial approximations of the longitudinal and transverse form factors. Each of these form factors was then fitted as a function of q with an extended oscillator expression consisting of the product of a Gaussian function and polynomial in q^2, as described in Sec. IV A 1. The fitted parametrization of the largely transverse results was used to correct the approximate longitudinal form factor, and vice versa. The procedure was iterated until convergence was obtained. Data available from previous experimental investigations [8–12] were also utilized in these analyses. The model dependence of the procedure was estimated by varying the degree of the polynomial term in the fitted form-factor expression. In general the model dependence was small, in large part as a result of the general dominance of longitudinal components in the data and the further dominance of a single longitudinal multipole, the $C2$. Two exceptions were the pure $M3$ form factor for the transition to the 1.740 MeV J^π=0$^+$, T=1 state, for which Rosenbluth separation was unnecessary, and the form factor for the 5.164 MeV excitation, which is also $M3$ dominated. Table I lists the longitudinal and transverse form factors determined for all excitations analyzed in this experiment.

The longitudinal and transverse form factors consist of incoherent sums over allowed multipoles λ:

$$F_L^2 = \sum_{\lambda=\lambda_{\min},2}^{\lambda_{\max}} F_{C\lambda}^2,$$

$$F_T^2 = \sum_{\lambda=\lambda_{\min}}^{\lambda_{\max}} \left[F_{E\lambda}^2 + F_{M\lambda}^2\right] ,$$

where the form-factor subscripts C and E indicate the

TABLE I. Longitudinal and transverse form factors deduced for low-energy transitions in ^{10}B. Percentage uncertainties are shown in parentheses. Only the form factors for the ground state and 1.740 MeV level have been corrected for Coulomb distortion, and these are listed as functions of the momentum transfer q, given in units of fm^{-1}; all other form factors are tabulated against effective momentum transfer $q_{\rm eff}$.

0.000 MeV $J^\pi = 3^+,\ T = 0$

q	F_L^2	q	F_L^2	q	F_L^2	q	F_L^2
0.48	5.79×10^{-1} (2.2)	0.79	2.61×10^{-1} (2.2)	0.94	1.54×10^{-1} (3.5)	1.13	7.55×10^{-2} (4.3)
1.19	5.23×10^{-2} (3.7)	1.39	2.12×10^{-2} (3.7)	1.59	8.52×10^{-3} (3.7)	1.75	3.74×10^{-3} (4.1)
1.79	2.95×10^{-3} (3.7)	1.95	1.63×10^{-3} (2.5)	1.98	1.27×10^{-3} (3.7)	2.09	9.47×10^{-4} (3.4)
2.18	6.02×10^{-4} (3.8)	2.58	1.11×10^{-4} (12.7)				

0.718 MeV $J^\pi = 1^+,\ T = 0$

$q_{\rm eff}$	F_L^2	$q_{\rm eff}$	F_L^2	$q_{\rm eff}$	F_L^2	$q_{\rm eff}$	F_L^2
0.49	5.92×10^{-6} (2589)	0.58	2.62×10^{-4} (7.2)	0.80	4.25×10^{-4} (6.2)	0.96	5.78×10^{-4} (4.5)
1.10	5.33×10^{-4} (12.7)	1.18	5.87×10^{-4} (5.2)	1.20	5.92×10^{-4} (15.1)	1.29	5.37×10^{-4} (5.0)
1.40	3.90×10^{-4} (8.7)	1.60	3.02×10^{-4} (6.7)	1.80	1.66×10^{-4} (6.1)	1.99	8.79×10^{-5} (5.8)
2.19	3.17×10^{-5} (9.3)	2.39	9.15×10^{-6} (30.9)	2.59	6.19×10^{-6} (63.1)		
$q_{\rm eff}$	F_T^2	$q_{\rm eff}$	F_T^2	$q_{\rm eff}$	F_T^2	$q_{\rm eff}$	F_T^2
0.80	-8.01×10^{-8} (4600)	1.15	3.37×10^{-5} (42.4)	1.34	1.84×10^{-5} (22.6)	1.48	2.32×10^{-5} (58.6)
1.67	1.13×10^{-5} (51.7)	1.77	1.64×10^{-5} (37.6)	1.86	1.14×10^{-5} (18.0)	1.97	5.74×10^{-6} (35.6)
2.11	7.11×10^{-6} (16.4)						

1.740 MeV $J^\pi = 0^+,\ T = 1$

q	F_T^2	q	F_T^2	q	F_T^2	q	F_T^2
0.56	9.22×10^{-6} (93.4)	0.78	3.01×10^{-5} (65.8)	0.77	3.74×10^{-5} (5.0)	0.94	5.30×10^{-5} (11.5)
1.08	9.46×10^{-5} (40.6)	1.12	1.25×10^{-4} (5.3)	1.17	1.24×10^{-4} (10.3)	1.19	1.79×10^{-4} (42.5)
1.27	1.42×10^{-4} (5.0)	1.31	1.52×10^{-4} (4.6)	1.39	2.24×10^{-4} (13.9)	1.45	1.65×10^{-4} (4.8)
1.59	1.58×10^{-4} (10.3)	1.65	1.50×10^{-4} (4.9)	1.75	1.47×10^{-4} (4.9)	1.78	1.39×10^{-4} (6.8)
1.83	1.48×10^{-4} (6.3)	1.94	1.28×10^{-4} (3.2)	1.98	1.02×10^{-4} (5.3)	2.08	1.02×10^{-4} (3.5)
2.18	7.85×10^{-5} (5.8)	2.38	4.65×10^{-5} (16.7)	2.57	2.97×10^{-5} (15.6)		

2.154 MeV $J^\pi = 1^+,\ T = 0$

$q_{\rm eff}$	F_L^2	$q_{\rm eff}$	F_L^2	$q_{\rm eff}$	F_L^2	$q_{\rm eff}$	F_L^2
0.49	3.57×10^{-5} (234)	0.58	6.68×10^{-5} (18.4)	0.79	1.53×10^{-4} (9.2)	0.95	1.85×10^{-4} (6.3)
1.10	2.30×10^{-4} (19.3)	1.18	2.41×10^{-4} (6.5)	1.20	2.20×10^{-4} (24.0)	1.28	2.32×10^{-4} (6.1)
1.40	2.25×10^{-4} (10.5)	1.60	1.52×10^{-4} (8.4)	1.79	8.72×10^{-5} (7.8)	1.99	4.85×10^{-5} (7.2)
2.19	2.32×10^{-5} (10.5)	2.39	3.86×10^{-6} (54.1)	2.59	1.05×10^{-6} (333)		
$q_{\rm eff}$	F_T^2	$q_{\rm eff}$	F_T^2	$q_{\rm eff}$	F_T^2	$q_{\rm eff}$	F_T^2
0.79	8.41×10^{-6} (20.8)	1.14	2.69×10^{-5} (25.9)	1.33	1.72×10^{-5} (14.6)	1.47	1.69×10^{-5} (44.9)
1.67	9.00×10^{-6} (42.4)	1.77	1.05×10^{-5} (36.3)	1.86	1.23×10^{-5} (11.9)	1.96	9.34×10^{-6} (18.1)
2.10	8.35×10^{-6} (15.2)						

3.587 MeV $J^\pi = 2^+,\ T = 0$

$q_{\rm eff}$	F_L^2	$q_{\rm eff}$	F_L^2	$q_{\rm eff}$	F_L^2	$q_{\rm eff}$	F_L^2
0.49	1.25×10^{-4} (55.6)	0.57	9.22×10^{-5} (10.5)	0.79	1.90×10^{-4} (6.5)	0.95	2.69×10^{-4} (4.8)
1.09	2.46×10^{-4} (15.0)	1.17	2.78×10^{-4} (5.7)	1.20	3.00×10^{-4} (17.2)	1.28	2.69×10^{-4} (5.2)
1.39	2.60×10^{-4} (9.0)	1.47	2.15×10^{-4} (6.1)	1.59	2.25×10^{-4} (6.7)	1.79	1.10×10^{-4} (6.9)
1.99	6.33×10^{-5} (6.3)	2.19	3.75×10^{-5} (14.5)	2.38	1.61×10^{-5} (44.7)	2.58	5.27×10^{-6} (51.0)
$q_{\rm eff}$	F_T^2	$q_{\rm eff}$	F_T^2	$q_{\rm eff}$	F_T^2	$q_{\rm eff}$	F_T^2
0.79	8.68×10^{-7} (188)	1.14	1.81×10^{-5} (41.6)	1.32	1.23×10^{-5} (19.8)	1.66	1.09×10^{-5} (36.0)
1.76	9.85×10^{-6} (43.3)	1.85	8.97×10^{-6} (18.2)	1.96	5.95×10^{-6} (29.8)	2.09	8.94×10^{-6} (13.4)

4.774 MeV $J^\pi = 3^+,\ T = 0$

$q_{\rm eff}$	F_L^2	$q_{\rm eff}$	F_L^2	$q_{\rm eff}$	F_L^2	$q_{\rm eff}$	F_L^2
0.49	-6.39×10^{-7} (9374)	0.57	7.64×10^{-5} (11.4)	0.79	1.30×10^{-4} (8.1)	0.95	1.80×10^{-4} (5.4)
1.09	1.71×10^{-4} (19.2)	1.17	1.36×10^{-4} (7.7)	1.20	1.17×10^{-4} (32.5)	1.27	1.05×10^{-4} (7.3)
1.39	6.93×10^{-5} (19.6)	1.46	5.66×10^{-5} (16.0)	1.59	3.10×10^{-5} (20.7)	1.79	1.49×10^{-5} (21.5)
1.98	4.90×10^{-6} (27.4)	2.18	2.01×10^{-6} (49.2)	2.38	4.19×10^{-7} (189)	2.58	1.42×10^{-6} (69.0)
$q_{\rm eff}$	F_T^2	$q_{\rm eff}$	F_T^2	$q_{\rm eff}$	F_T^2	$q_{\rm eff}$	F_T^2
1.13	8.89×10^{-6} (53.0)	1.32	9.16×10^{-6} (15.2)	1.66	2.12×10^{-6} (82.2)	1.76	4.73×10^{-6} (32.8)

TABLE I. *(Continued).*

1.84	3.53×10^{-6} (13.3)	1.95	1.83×10^{-6} (40.7)	2.09	1.14×10^{-6} (48.4)		
5.110 MeV		$J^\pi = 2^-,\ T = 0$					
q_{eff}	F_L^2	q_{eff}	F_L^2	q_{eff}	F_L^2	q_{eff}	F_L^2
0.57	1.68×10^{-5} (50.0)	0.79	8.19×10^{-5} (12.8)	0.94	1.81×10^{-4} (5.8)	1.09	1.72×10^{-4} (21.7)
1.17	2.35×10^{-4} (6.9)	1.19	1.96×10^{-4} (25.7)	1.27	2.02×10^{-4} (6.4)	1.39	1.38×10^{-4} (17.6)
q_{eff}	F_T^2	q_{eff}	F_T^2				
1.13	8.90×10^{-6} (89.9)	1.32	4.39×10^{-5} (11.0)				
5.164 MeV		$J^\pi = 2^+,\ T = 1$					
q_{eff}	F_L^2	q_{eff}	F_L^2	q_{eff}	F_L^2	q_{eff}	F_L^2
0.49	1.08×10^{-5} (528)	0.79	-1.90×10^{-5} (89.6)	1.17	2.54×10^{-5} (158)	1.19	3.00×10^{-5} (187)
1.39	4.97×10^{-5} (75.9)						
q_{eff}	F_T^2	q_{eff}	F_T^2	q_{eff}	F_T^2	q_{eff}	F_T^2
0.57	3.44×10^{-5} (19.5)	0.94	1.84×10^{-4} (9.2)	1.09	2.98×10^{-4} (13.2)	1.13	3.04×10^{-4} (5.6)
1.27	3.94×10^{-4} (5.5)	1.32	4.18×10^{-4} (4.5)	1.76	4.43×10^{-4} (4.8)		
Unresolved 5.1 MeV complex							
q_{eff}	F_L^2	q_{eff}	F_L^2	q_{eff}	F_L^2	q_{eff}	F_L^2
1.59	1.45×10^{-4} (45.4)	1.79	5.78×10^{-5} (105)	1.98	8.09×10^{-6} (589)	2.18	1.72×10^{-5} (206)
2.38	7.61×10^{-7} (6145)	2.58	1.05×10^{-5} (930)				
q_{eff}	F_T^2	q_{eff}	F_T^2	q_{eff}	F_T^2	q_{eff}	F_T^2
1.46	4.88×10^{-4} (5.0)	1.65	4.77×10^{-4} (3.3)	1.84	4.47×10^{-4} (3.7)	1.95	4.01×10^{-4} (2.9)
2.09	2.90×10^{-4} (7.7)						
5.920 MeV		$J^\pi = 2^+,\ T = 0$					
q_{eff}	F_L^2	q_{eff}	F_L^2	q_{eff}	F_L^2	q_{eff}	F_L^2
0.79	5.33×10^{-5} (16.9)	0.94	8.77×10^{-5} (7.5)	1.08	9.03×10^{-5} (15.4)	1.13	9.13×10^{-5} (7.3)
1.17	1.05×10^{-4} (9.0)	1.19	9.55×10^{-5} (34.1)	1.27	1.17×10^{-4} (11.8)	1.39	6.98×10^{-5} (23.3)
1.46	5.88×10^{-5} (29.6)	1.59	5.20×10^{-5} (19.0)	1.65	5.59×10^{-5} (36.1)	1.75	1.59×10^{-5} (53.9)
q_{eff}	F_T^2	q_{eff}	F_T^2	q_{eff}	F_T^2	q_{eff}	F_T^2
1.31	2.89×10^{-6} (59.7)	1.84	5.42×10^{-6} (45.9)	1.95	7.37×10^{-6} (39.1)	2.08	5.77×10^{-6} (31.0)
6.025 MeV		$J^\pi = 4^+,\ T = 0$					
q_{eff}	F_L^2	q_{eff}	F_L^2	q_{eff}	F_L^2	q_{eff}	F_L^2
0.48	1.50×10^{-3} (7.3)	0.79	5.47×10^{-3} (2.3)	0.94	7.55×10^{-3} (3.7)	1.08	7.92×10^{-3} (3.7)
1.13	7.89×10^{-3} (4.7)	1.17	7.95×10^{-3} (3.6)	1.19	7.42×10^{-3} (4.7)	1.27	8.03×10^{-3} (4.4)
1.39	6.77×10^{-3} (3.9)	1.46	5.62×10^{-3} (5.1)	1.59	4.35×10^{-3} (3.9)	1.65	3.81×10^{-3} (4.9)
1.75	2.88×10^{-3} (4.4)	1.79	2.65×10^{-3} (4.0)	1.98	1.28×10^{-3} (3.9)	2.18	4.37×10^{-4} (4.5)
2.38	1.23×10^{-4} (15.4)	2.58	1.89×10^{-5} (26.5)				
q_{eff}	F_T^2	q_{eff}	F_T^2	q_{eff}	F_T^2	q_{eff}	F_T^2
1.31	8.47×10^{-5} (51.6)	1.84	1.60×10^{-5} (124)	1.95	4.86×10^{-5} (26.8)	2.08	6.66×10^{-6} (71.0)
6.127 MeV		$J^\pi = 3^-,\ T = 0$					
q_{eff}	F_L^2	q_{eff}	F_L^2	q_{eff}	F_L^2	q_{eff}	F_L^2
0.48	4.64×10^{-5} (128)	0.79	1.25×10^{-4} (12.1)	0.94	2.71×10^{-4} (6.9)	1.08	5.06×10^{-4} (18.8)
1.13	3.76×10^{-4} (7.7)	1.17	4.48×10^{-4} (6.5)	1.19	4.04×10^{-4} (25.7)	1.27	3.91×10^{-4} (6.4)
1.39	4.15×10^{-4} (12.8)	1.46	6.08×10^{-4} (7.4)	1.59	4.10×10^{-4} (8.1)	1.65	3.62×10^{-4} (7.4)
1.75	2.05×10^{-4} (9.2)	1.95	8.88×10^{-5} (28.5)				
q_{eff}	F_T^2	q_{eff}	F_T^2	q_{eff}	F_T^2		
1.31	7.68×10^{-6} (72.2)	1.84	5.76×10^{-6} (92.4)	2.08	1.64×10^{-6} (191)		
6.561 MeV		$J^\pi = 4^-,\ T = 0$					
q_{eff}	F_L^2	q_{eff}	F_L^2	q_{eff}	F_L^2	q_{eff}	F_L^2
0.48	2.13×10^{-5} (277)	0.79	9.09×10^{-5} (34.1)	0.94	1.91×10^{-4} (27.2)	1.08	2.63×10^{-4} (24.3)
1.17	2.64×10^{-4} (6.0)	1.19	2.77×10^{-4} (21.9)	1.27	2.95×10^{-4} (5.0)	1.39	2.94×10^{-4} (10.1)
1.46	2.42×10^{-4} (11.6)	1.59	2.78×10^{-4} (7.8)	1.78	1.60×10^{-4} (7.1)	1.98	8.17×10^{-5} (6.2)
2.18	3.81×10^{-5} (9.2)	2.38	1.87×10^{-5} (20.6)	2.58	6.47×10^{-6} (27.7)		
q_{eff}	F_T^2	q_{eff}	F_T^2	q_{eff}	F_T^2	q_{eff}	F_T^2
1.12	3.08×10^{-5} (62.0)	1.31	1.29×10^{-5} (34.8)	1.65	2.51×10^{-7} (1994)	1.75	4.02×10^{-6} (153)
1.84	9.85×10^{-7} (149)	1.95	3.33×10^{-7} (789)				

charge and current parts of electric multipoles, and M specifies magnetic multipoles. For these types of data the contributions of individual multipoles are not explicitly manifested, but nuclear models are often instructive in providing an understanding of the multipole composition of deduced longitudinal and transverse form factors.

III. THEORY

A. Historical background

Attempts to describe the properties of ^{10}B in terms of the microscopic shell model date back to the infancy of this model, some 40 years ago [20]. At least two different methods have been used to construct effective two-body interactions for $1p$-shell nuclei. The best-known example of the main approach is the work of Cohen and Kurath [21], who obtained two-body matrix elements and single-particle energies by fitting the energies of selected levels in $1p$-shell nuclei. In the case of ^{10}B, however, these interactions give wrong signs for the $E2/M1$ mixing ratios in radiative decays of low-lying $J=1^+$ and 2^+ states [22]. A subsequent reinterpretation by Kurath [23] showed that the signs could be corrected by asserting the dominance of the $L=4$, $K_L=2$ component in the LS representation of the ^{10}B wave functions. This suggestion was further developed by Barker [24], who modified the two-body matrix elements of Cohen and Kurath to obtain two sets of interaction parameters that are more successful not only for ^{10}B, but also for the neighboring $A=9$ and $A=11$ nuclei.

In the second, more fundamental, approach the effective two-body interaction is constructed directly from observed free NN scattering phase shifts. An advantageous simplification is provided by the Sussex version [25] of this method, whereby the two-body matrix elements are obtained without the need to formulate an explicit expression for the interaction. Most applicable to the case of ^{10}B are the results of Hauge and Maripuu [26] who evaluated $2\hbar\omega$ corrections to the "bare" Sussex matrix elements by means of second-order perturbation theory. The resultant effective interactions were then used in shell-model calculations for $A=6$–14 nuclei.

Both these approaches lead to predictions that are in good agreement with the observed spectra of natural-parity levels, as represented in Fig. 2 by the example of the Cohen and Kurath (8-16)2BME interaction [21]. Similarly impressive predictions are given for magnetic dipole moments, $M1$ transition widths, and Gamow-Teller β-decay rates [21,24,26]. In other respects, however, most notably but not exclusively with regard to electric multipole moments and transition rates, these $1p$-shell models consistently fail. In part, these problems may stem from fundamental limitations. For example, effective $1p$-shell matrix elements determined using the method of Cohen and Kurath are valid only to the extent that the fitted nuclear levels have properties that are primarily determined by $1p$-shell configurations; the presence of large $(2s1d)^2$ admixtures, for instance, could modify appreciably the deduced matrix elements. Furthermore, the adequacy of theoretical methods used to construct effective matrix elements from free NN scattering phase shifts remains to be proved.

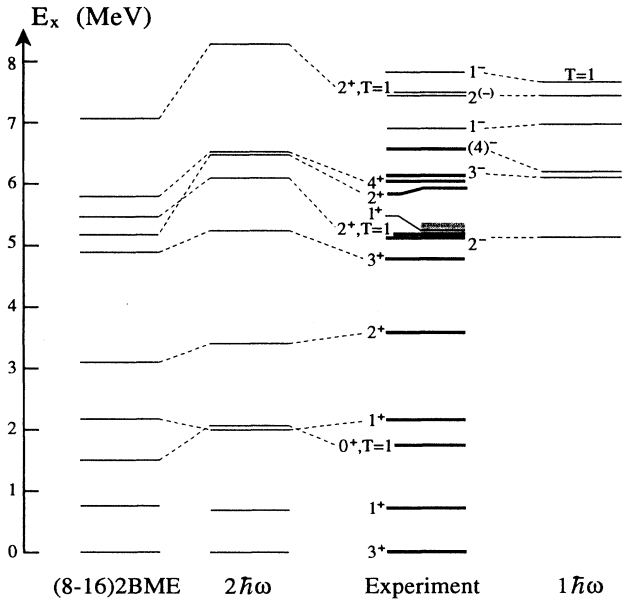

FIG. 2. Comparison of observed and theoretical spectra of low-lying states in ^{10}B. States for which form factors were measured are indicated in the experimental spectrum by heavy lines.

B. $1\hbar\omega$ and $2\hbar\omega$ shell-model calculations

Even with these reservations, it is clear that the shortcomings of the models stem mainly from the restriction of the shell-model basis space to the $1p$ shell. As a first step towards solving this problem the shell-model basis space was expanded to include $1\hbar\omega$ and $2\hbar\omega$ configurations that have holes in the $1s$ shell or particles in the $2s1d$ and $2p1f$ shells. For the cross-shell interaction we used that of Millener and Kurath [27]. Figure 2 shows the calculated spectrum of even-parity levels to be in acceptable agreement with the experimental observations, although not as favorably as the results of the $1p$-shell calculation. In particular, the $2\hbar\omega$ calculation positions the $T=1$ states too high.

Inclusion of the $1s$ and $2s1d$ shells is, of course, essential for understanding states of unnatural parity. A slightly modified version of the Millener-Kurath interaction yields the spectrum of $1\hbar\omega$ states shown on the right of Fig. 2. The agreement with the observed odd-parity spectrum is excellent, confirming the results of a previous shell-model calculation [28] that utilized different, empirically determined, interactions.

In the range of our measurements, the 1^+ level at 5.18 MeV is the only recognized level without a counterpart in the shell-model spectra. Perhaps not coincidentally, below 6.7 MeV this was the only excitation for which our experiment failed to find evidence. This suggests a more complex structure for the 5.18 MeV level than can

be given by a restricted shell model, and indeed, this level is predicted by the $(2\alpha + d)$ cluster-model calculation of Nishioka [29]. A cluster-model interpretation for this level is also suggested by its large observed width in ^{6}Li+α elastic scattering [30].

As will be seen, even with $2\hbar\omega$ configurations, the shell model is still hard pressed to account for the more collective properties of the nucleus, and further expansions of the basis space beyond $2\hbar\omega$ unfortunately become extremely cumbersome using standard techniques.

C. Core polarization

Perturbative core-polarization calculations provide a more practical alternative for evaluating nuclear collectivity. In the extended shell model, first-order core polarization is a coherent superposition of single-particle matrix elements involving particles in highly excited shells. Sato *et al.* [7] have recently published detailed calculations of the effects of core polarization on (e,e'), (π,π'), and (γ,π) cross sections for ^{10}B. In first-order perturbation theory the matrix element of the one-body operator $\mathcal{O}_J$ for a transition between $1p$-shell states $|J_i\rangle$ and $|J_f\rangle$ may be expressed as the sum of three terms, a $1p$-shell part and two core-polarization matrix elements [31]:

$$\langle J_f|\mathcal{O}_J|J_i\rangle + \left\langle J_f \left| \mathcal{O}_J \frac{Q}{E_i - H_0} V_{\rm res} \right| J_i \right\rangle + \left\langle J_f \left| V_{\rm res} \frac{Q}{E_f - H_0} \mathcal{O}_J \right| J_i \right\rangle ,$$

where the Hamiltonian H_0 represents the shell-model mean field and Q is the projection operator onto the space outside the $1p$ shell. For the residual interaction $V_{\rm res}$, Sato *et al.* [31] used the M3Y potential of Bertsch *et al.* [32] which reproduces the Sussex matrix elements. In order for the calculations to converge it was found necessary to include core polarization configurations up to $6\hbar\omega$ above the p shell.

Because previous (e,e') data existed for just four transitions in ^{10}B, Sato *et al.* were able to make only a limited comparison with experiment. The biggest core-polarization contribution was obtained for the $C2$ multipoles of the elastic and 6.025 MeV inelastic form factors. Particularly in the latter case, where the $1p$-shell predictions were increased by a factor of 2.6, enhancements due to core polarization were essential in bringing the theoretical results into quantitative agreement with the data. It was found [7] that such agreement could not be obtained by performing calculations within a restricted $1p$-shell space and utilizing state-independent "effective charges" for the nucleons. Smaller, but nonetheless important, core-polarization effects were also observed for $M3$ form factors of the 1.740 and 5.160 MeV transitions.

IV. RESULTS AND INTERPRETATION

A. Elastic form factor and the ground-state charge distribution

1. Phenomenological interpretation

For the kinematics of this experiment, longitudinal scattering was overwhelmingly dominant in the cross section for elastic scattering from ^{10}B. Small magnetic components in the data were assessed by means of a fit to previous experimental results [2] obtained mostly at θ=180°. Because these corrections were always less than 3%, adequate accuracy was obtained using the simple $q_{\rm eff}$ transformation described in Sec. IV B 1 to account for the Coulomb distortion of the magnetic form factor. Although the deduced charge factor, shown in Fig. 3, is composed of an incoherent sum of $C0$, $C2$, $C4$, and $C6$ multipoles, theory predicts that the $C4$ and $C6$ contributions are negligible for the momentum transfer range of this experiment. The remaining $C0$ and $C2$ multipole contributions can only be separated using models for the ground-state monopole and quadrupole charge densities. The isolation of the $C0$ form factor is of special interest since it is a transform of the ground-state charge density $\rho(r)$:

$$F_{C0} = \int_0^\infty \rho(r) j_0(qr) r^2 dr \ .$$

A previous measurement of elastic electron scattering from ^{10}B was made at Orsay by Stovall *et al.* [12] who fitted the $M1$-corrected results to obtain the rms charge radius and ground-state quadrupole moment. Spherical and deformed oscillator models were used. Only the spherical oscillator gave an acceptable fit, corresponding to an rms charge radius of 2.45 ± 0.12 fm and quadrupole

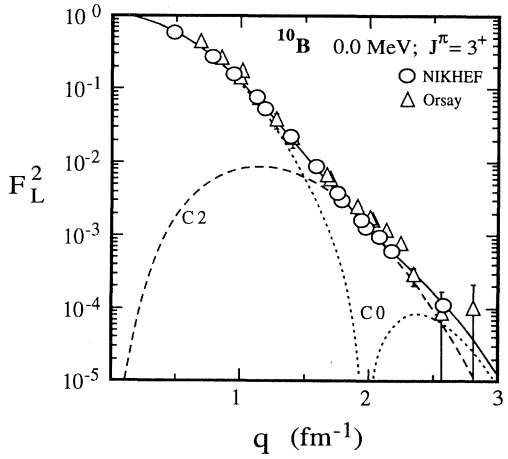

FIG. 3. Charge form factor for elastic scattering from ^{10}B. The data, which have been corrected for Coulomb distortion, are from the present experiment (NIKHEF) and Ref. [12] (Orsay). As described in the text, the curves result from a fit to the data; the $C0$ and $C2$ components are identified; the solid curve is the sum.

moment $Q = 7.45 \pm 1.5$ fm^2. These values agree with later results of 2.44 ± 0.06 fm for the rms size, from a muonic x-ray experiment [33], and $Q = 8.472 \pm 0.056$ fm^2, from the atomic hyperfine interaction [34]. The relatively large uncertainties in the electron-scattering results were attributed [12] mainly to the model dependence of separating the $C0$ and $C2$ form-factor components.

Form-factor values deduced by Stovall are included in Fig. 3. In general, these agree with the present results, but the 20–50% errors are much larger than the uncertainties in the present data, which are $< 4\%$ except at the highest q. Although we were able to reproduce the results of the spherical-oscillator analysis of Stovall *et al.*, it has been shown [2] that the oscillator provides a poor representation of the radial dependence of the $1p_{3/2}$ orbit in ^{10}B. In particular, this model predicts a $1p_{3/2}$ density that decreases much too quickly at large nuclear radii. Since roughly three of the five ^{10}B protons will occupy $1p_{3/2}$ orbits, oscillator wave functions should also be inappropriate for calculating the elastic charge form factors. This expectation was confirmed by least-squares fits to the new, more precise, elastic data.

Our first analyses of the data used a q_{eff} transformation to account for Coulomb distortion of the incoming and outgoing electron waves. Using the deduced charge densities, full DWBA calculations were iterated to yield correction factors for removing Coulomb distortion from the data. It is these "plane-wave" form-factor values that are shown in Fig. 3. The curves in Fig. 3 are the result of a fit which has a $C0$ component derived from the simple two-parameter Fermi model of the nuclear charge density:

$$\rho(r) \propto \{1 + \exp[(r-c)/z]\}^{-1} \ ,$$

where the half-density radius c and diffuseness z were fitted parameters. Provided z is not too small, this expression gives near the nuclear periphery a larger charge density than is provided by the oscillator representation. The χ^2 value for this fit, 1.2 per degree of freedom, is 2 times better than the results of fits based on the harmonic-oscillator $C0$ expression.

In contrast, the overall quality of the fits proved to be relatively insensitive to the parametrization of the $C2$ component. The $C2$ curve shown in Fig. 3 merely follows the $1p$-shell harmonic-oscillator dependence, which, excluding nucleon finite size and center-of-mass corrections, is given by [12]

$$F_{C2} = 0.0231 Q^2 q^2 e^{-y} \ , \tag{3}$$

where $y = b^2q^2/4$. In the analysis of the Orsay results, Stovall *et al.* forced the value of the oscillator size parameter b to equal that of the $C0$ component, a constraint of doubtful validity due to the recognized sensitivity of $C2$ form factors to core polarization. (For the ^{10}B ground state the importance of core polarization is already evident from $1p$-shell model calculations [21,24] that give only half the observed quadrupole moment of Q=8.472 fm^2.) Support for the use of the harmonic-oscillator $C2$ expression comes from our measurements of transitions to the ^{10}B excited states at 0.718, 2.154, 3.587, 4.774, and 6.025 MeV. As will be shown, the associated form factors have longitudinal components which are all dominated by the $C2$ multipole. Notwithstanding clear contributions from core polarization, most of these form factors could be adequately fit by the $1p$-shell oscillator expression provided that the oscillator size parameter b was permitted to be a free parameter.

Before presenting the quantitative results of this analysis, some consideration is required of the model dependence of the interpretation. With regard to the $C2$ component, for example, it was observed that the quality of the harmonic-oscillator fits to the *inelastic* $C2$ form factors was somewhat improved when the oscillator polynomial was expanded to cubic order in q^2, i.e.,

$$F_{C2} = e^{-y}\left(a_0 y + a_1 y^2 + a_2 y^3\right) \ . \tag{4}$$

(The average χ^2 value per degree of freedom decreased from 1.46 to 1.05.) The expansion of the harmonic-oscillator expression in this way is equivalent to expanding the model space beyond the $1p$ shell.

Based on this observation, three contrasting representations were used to fit the $C2$ part of the elastic form factor, each of which utilized the oscillator size parameter b as a variable parameter:

(A) A simple $1p$-shell expression given in Eq. (3) with Q fixed to the observed value of 8.472 fm^2. This result has already been presented in Fig. 3.

(B) A simple $1p$-shell expression given in Eq. (3) with Q freely varied. The justification for this approach is that in (e,e') the value of Q is strictly manifested only by the slope of the $C2$ form factor at low q, a region where our results are dominated by the $C0$ multipole. Figure 3 shows that in the present case the $C2$ multipole is important only above q=1.5 fm^{-1}. The freeing of Q to be fitted is tantamount to the admission that the $C2$ form factor need not have a strict $1p$-shell oscillator dependence over all q.

(C) An extended expression given by Eq. (4), with the coefficients a_0, a_1, and a_2 as free parameters.

The final results of these three analyses are compared in Figs. 4 and 5. Per degree of freedom, the χ^2 values for these fits range from 1.17 to 1.21, so that all three $C2$ models give similarly good fits to the data. Figure 4 shows the range spanned by the three fitted $C0$ and $C2$ components. Irrespective of the $C2$ model, the $C0$ form factor is isolated below q=1.1 fm^{-1}, while the $C2$ contribution is dominant near q=2 fm^{-1}. Elsewhere, the primary multipole character of the data is unclear. As far as the $C0$ form factor is concerned, then, the data above $q \approx 1.5$ fm^{-1} serve only to define an upper limit. Nonetheless, although values obtained for the half-density radius c and diffuseness z varied appreciably from fit to fit, the corresponding rms size of the ground-state charge density remained relatively stable, varying by only $\pm 1\%$.

The somewhat flattened diffraction shape obtained for the cubic polynomial $C2$ (model C) fit was not seen in the data for any of the five inelastic $C2$ transitions listed above. This anomalous shape is a reflection of the looseness of the fit constraints and suggests that the cubic

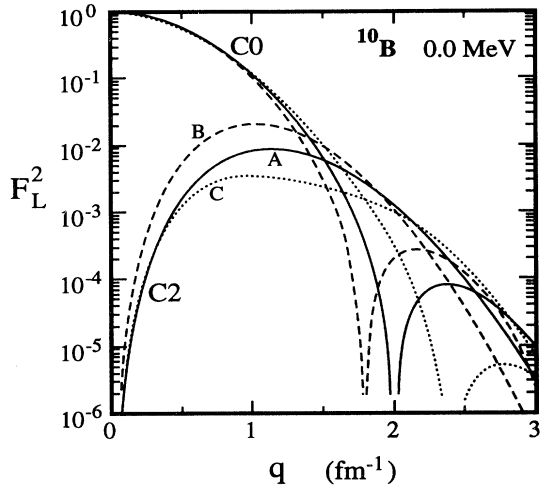

FIG. 4. $C0$ and $C2$ components resulting from three fits to the ^{10}B charge form factor, as described in the text.

polynomial model provides a lower limit to the $C2$ component in the range $0.5 < q < 2$ fm^{-1}. Similarly, with a fitted quadrupole moment almost twice the observed value, the result based on the second $C2$ model [model (B)] could be considered as an upper limit to the $C2$ component below q=1.5 fm^{-1}. We therefore feel that model (B) and (C) curves set conservative bounds on the interpretation below $q \approx 2$ fm^{-1}.

Also required is some consideration of the dependence of the interpretation on the $C0$ model. Offerman *et al.* [18], for example, have presented evidence for a slight depression in the central charge density of ^{12}C, an effect that lies beyond the scope of the two-parameter Fermi

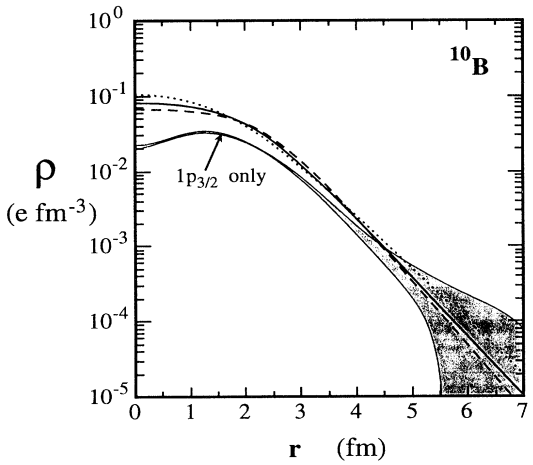

FIG. 5. Ground-state charge densities of ^{10}B, derived from three separate $C2$ models as described in the text. The solid curve is for model (A), dashed curve for model (B), and dotted curve for model (C). The shaded band represents the $1p_{3/2}$ density obtained from a Fourier-Bessel analysis of the $M3$ form factor for the 1.74 MeV transition, normalized to a $1p_{3/2}$-shell occupancy of three protons. The proton size is included in all curves.

model discussed above. Depressions or augmentations in the central charge density can be introduced by means of a "wine-bottle" parameter w:

$$\rho(r) \propto \frac{\left[1 + \left(wr^2/c^2\right)\right]}{1 + \exp\left[(r-c)/z\right]} .$$

While the nature and quality of the ^{10}B elastic results prevent a useful determination of the value of w, analyses using this three-parameter Fermi model provided a practical means of estimating the uncertainty due to model dependence. In summary, our final result for the rms size of the ^{10}B charge density is $2.58 \pm 0.05 \pm 0.05$ fm, where the first error represents the statistical uncertainty, and the second error is the estimated systematic uncertainty due to the model dependence of the $C0$ and $C2$ form factors. Experimental systematic uncertainties, such as those associated with the overall normalization of the data or incident beam energy, are relatively small.

The increase in this rms size over the 2.45 ± 0.12 fm obtained by Stovall *et al.* [12] does not reflect a discrepancy between the present and older Orsay data; indeed, separate fits to the individual data sets yield rms sizes that are essentially identical. The larger rms size derives almost entirely from what we have argued is a more appropriate parametrization of the ground-state charge density. The oscillator model used by Stovall *et al.* predicts a density which decreases too quickly at the nuclear surface. Since this contribution is heavily weighted in the computation of the rms size, the harmonic-oscillator analysis gives a rms size that is too small [35].

The new (e,e') result for the rms charge radius is just marginally consistent with the value of 2.44 ± 0.06 fm obtained by Olin *et al.* [33] from measurements of muonic x-ray energy shifts. Although the analysis of Olin *et al.* relied upon oscillator wave functions, the uncertainty assigned to their result includes an estimated contribution due to the model dependence of the charge distribution. On the basis of results obtained for ^{12}C, better agreement might have been expected. For example, a global analysis of elastic ^{12}C(e,e') measurements by Offerman *et al.* [18] yielded an rms size for the ^{12}C ground state of $2.476^{+0.007}_{-0.011}$ fm. A small calculated correction for dispersion effects increased this value to 2.483 fm, a value in perfect agreement with the 2.4829 ± 0.0019 fm obtained from a very precise muonic x-ray experiment [36].

What is determined in the muonic x-ray measurements is simply a moment of the ground-state charge distribution; in principle, elastic electron scattering provides more detailed information on the radial dependence of the charge. Figure 5 shows the charge distributions obtained from fits to the (e,e') measurements using the three different $C2$ models. Despite differences in the nuclear interior, the deviations between the densities for $r > 1.5$ fm are not large. These charge distributions are compared to results to be presented later for the $1p_{3/2}$ density, obtained by Fourier-Bessel analysis of the 1.74 MeV $M3$ form factor. The normalization of the ground-state charge distribution corresponds to five protons; in accordance with the extreme single-particle model, the $1p$-shell density is normalized to three protons. The com-

parison suggests that protons in the $1s$ shell (and perhaps other nonvalence orbits) constitute an important part of the charge distribution all the way out to r=4 fm, where the density has dropped to $\approx 2\%$ of that in the nuclear interior.

2. *Comparison with shell model*

In Fig. 6 experimental results on the elastic charge and magnetic form factors are compared to the results of $2\hbar\omega$ shell-model evaluations using Woods-Saxon and harmonic-oscillator radial wave functions. In the relative core-particle coordinate frame [37] the Woods-Saxon well parameters were R=1.17 $(A-1)^{1/3}$ fm for the radius and z=0.75 fm for the diffuseness. The $1s$- and $1p$-shell binding energies were set to -30 and -7 MeV, whereas -1 MeV was assumed for the $2s1d$ and higher shells. Spin-orbit splitting was neglected. The size parameter for the oscillator calculations was b=1.65 fm. In both cases these values give rms ground-state sizes of 2.50 fm, within the range of observed values. Considering that the charge form-factor data extend over almost four decades, the Woods-Saxon and oscillator predictions are both reasonably sound. Contributing to this overall success is the strengthening of the $C2$ form-factor component by $2\hbar\omega$ configurations, as indicated in the figure. At q=2.5 fm^{-1}, near the minimum in the $C0$ form factor, this increase amounts to approximately 60%.

The shell-model calculations are somewhat less successful for the magnetic form factor, where much of the data lie between the oscillator and Woods-Saxon curves. For $q < 2$ fm^{-1} the calculations predict that the $M1$ multipole dominates, and for this multipole the $1p$-shell and $2\hbar\omega$ results are almost identical. As has been previously

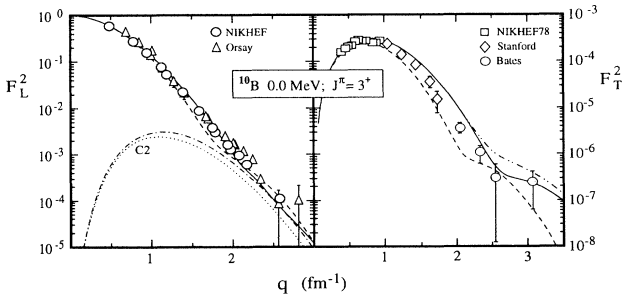

FIG. 6. Elastic form factors of ^{10}B and comparison with $2\hbar\omega$ shell-model calculations. The longitudinal data, which have been corrected for Coulomb distortion, are as shown in Fig. 3. The transverse measurements are simply plotted as a function of $q_{\rm eff}$, and come from Refs. [38] (NIKHEF78), [39] (Stanford), and [2] (Bates). The dashed curves indicate the sums of all contributing multipoles for oscillator (b=1.65 fm) radial wave functions. All remaining curves were obtained using Woods-Saxon wave functions: The solid curves are the multipole sums, whereas the dotted and dot-dashed curves show $C2$ contributions, the former for the (8-16)2BME $1p$-shell model and the latter for the $2\hbar\omega$ shell model. Also indicated, by the dash-double-dotted curve, is the (8-16)2BME $1p$-shell result for the magnetic form factor.

shown [2], the agreement can be improved by modifying the radial dimensions of the nuclear potential models, although this would spoil the correspondence between the predicted and observed values of the rms ground-state size. The objective, of course, is to seek a model which explains the charge and magnetic properties simultaneously, with the same potential parameters.

Figure 7 shows the core-polarization calculations for the charge and magnetic elastic form factors, obtained using oscillator wave functions with b=1.60 fm, the value adopted for elastic scattering in Ref. [7]. A notable result of core polarization is to increase the $C2$ component by a factor of 2.4 over the restricted $1p$-shell calculation, indicating that the $2\hbar\omega$ shell model is still too restrictive. Because it is obscured in the electron-scattering measurement, the clearest indication of the quadrupole component is the quadrupole moment. This is related to the $q = 0$ limit of the ^{10}B $C2$ form factor by

$$Q = \lim_{q\to 0} 43.3 q^{-2} F_{C2}(q) \ .$$

The three $1p$-shell interactions employed in this paper, the (8-16)2BME and (8-16)POT potentials of Cohen and Kurath and the Hauge-Maripuu potential, predict values for Q that are essentially the same: For oscillator wave functions with b=1.60 fm the result is Q=4.4 fm^2. With the inclusion of $2\hbar\omega$ configurations the prediction is raised to 5.0 fm^2, whereas the core-polarization calculations give Q = 7.8 fm^2, not far from the observed value of 8.472 fm^2. Overall then, the core-polarization model provides the most satisfactory description of the charge and magnetic form factors.

B. Strong $E2$ transitions

1. *Longitudinal form factors*

Figures 8 and 9 show the longitudinal form factors of transitions to T=0 even-parity states at 0.718 (J=1),

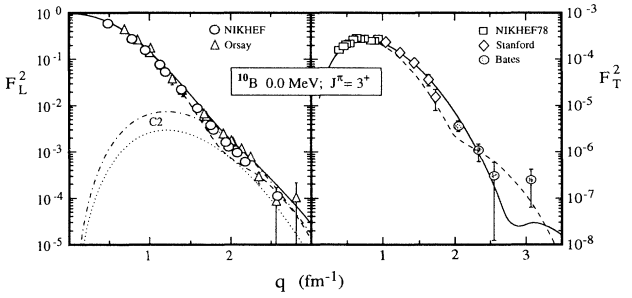

FIG. 7. Comparison of observed elastic form factors to the results of core-polarization calculations that use oscillator wave functions with b=1.60 fm. Dashed curves show $1p$-shell calculations based on the (8-16)POT potential; solid curves include first-order core polarization. All contributing multipoles are included. The remaining curves are for the $C2$ multipole only: The dotted curve is for the $1p$-shell model, whereas the dot-dashed curve includes core polarization. Almost identical results are obtained with the $1p$-shell density matrix elements of Hauge and Maripuu [26].

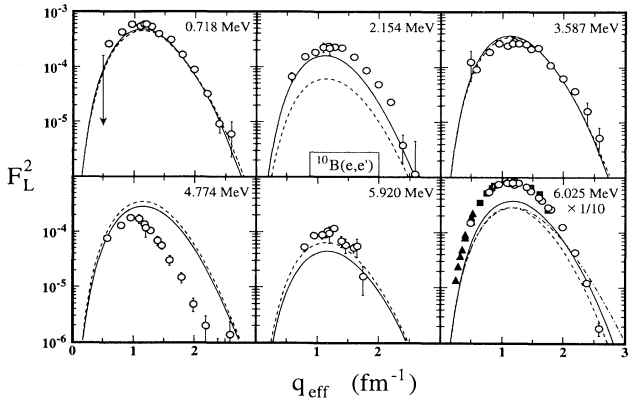

FIG. 8. Longitudinal form factors for mainly $C2$-dominated transitions to even-parity states in ^{10}B. In the measurements of Spamer [9] (triangles) and Ansaldo *et al.* [6] (squares) for the 6.025 MeV excitation this level was not resolved from the nearby 5.920 and 6.127 MeV states. All other points are from the present experiment. Dashed curves depict the results of shell-model calculations for the $C2$ multipole using the (8-16)2BME $1p$-shell interactions; solid curves indicate the $2\hbar\omega$ shell-model results. Although the $2\hbar\omega$ shell-model calculations include all possible multipoles, the $C2$ components were overwhelmingly dominant. All these calculations use oscillator wave functions with b=1.7 fm. For comparison, the dot-dashed curve shows the result of a $2\hbar\omega$ Woods-Saxon calculation for the 6.025 MeV transition. Note that both the data and the calculations for this transition have been multiplied by 1/10.

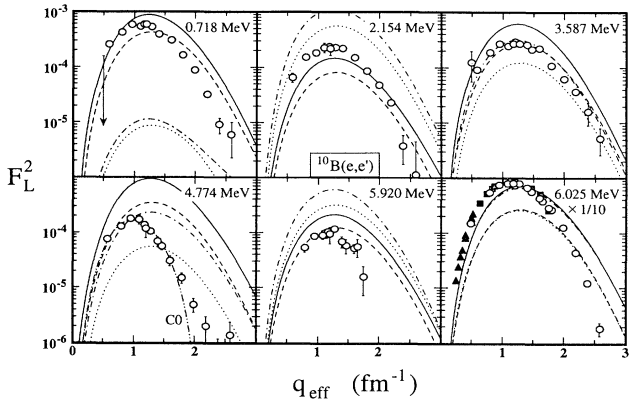

FIG. 9. Longitudinal form factors for $C2$-dominated transitions and comparison with core-polarization calculations. Dashed curves represent $1p$-shell calculations based on the (8-16)POT interaction; solid curves include core polarization. The dotted and dot-dashed curves are the corresponding results for the Hauge-Maripuu interaction. In each case the curves represent the sum of all possible multipole contributions, although the $C2$ multipole is dominant in the longitudinal form factors. Oscillator radial wave functions were used with b=1.5 fm. The dash–double-dotted curve shows the q dependence of the 8.66 MeV $C0$ form factor in ^{13}C, normalized to fit the 4.774 MeV ^{10}B data.

2.154 (J=1), 3.587 (J=2), 4.774 (J=3), 5.920 (J=2), and 6.025 (J=4) MeV. These results are plotted as a function of the "effective" momentum transfer [40], for the case of ^{10}B given by $q_{\rm eff} = q(1 + 2.75/E_0)$, where the beam energy E_0 is in MeV. The applicability of this expression, established by directly comparing theoretical form factors calculated in plane-wave and distorted-wave Born approximations, simplifies the comparison of the data with theoretical results.

Data previously acquired [6,9–11] on these transitions are almost exclusively limited to the triplet at 6.0 MeV, which was not resolved. This complex includes not only the 5.920 and 6.025 MeV levels, but also the J=3$^-$, 6.127 MeV state. Our good resolution measurements show that the longitudinal form factor of the 6.025 MeV excitation exceeds, by more than a factor of 15, the longitudinal form factors of either the 5.920 or 6.127 MeV transitions, or indeed any other transition shown in Fig. 8.

Also included in Fig. 8 are the results of shell-model calculations that use oscillator wave functions with b=1.70 fm, a value that is a reasonable compromise for these form factors. The calculations indicate that the 6.025 MeV form factor, as well as the form factors of the other transitions, is dominated by the $C2$ multipole component. For example, $C4$ form factors obtained in the $2\hbar\omega$ model space have form factors that typically peak two orders of magnitude below their $C2$ counterparts. Thus, although the $2\hbar\omega$ results shown in Fig. 8 include all allowed multipoles, the curves barely differ from the $C2$ form factors alone. Theoretical results are also presented for the $1p$-shell model. When harmonic-oscillator radial wave functions are employed, as is the case here, all $C2$ form factors should have identical q dependences in any $1p$-shell model. This prediction is only slightly compromised by the $2\hbar\omega$ calculations. The data are reasonably consistent with the calculated $C2$ q dependence except for the anomalous 4.774 MeV transition, which will be discussed later.

The comparison of the data to the predictions of both the $1p$-shell and $2\hbar\omega$ models provides a measure of the extent to which the collective enhancement of the $C2$ transitions can be attributed to $2\hbar\omega$ components. Figure 8 shows that the 0.718 and 3.587 MeV transitions do not require a large core-polarization effect: The data are in reasonable accord with the $1p$-shell calculations which are only slightly modified by the inclusion of $2\hbar\omega$ components. In the case of the 2.154 MeV transition, the $1p$-shell prediction underestimates the experimental results by a factor of 3, a disagreement that is largely remedied by the $2\hbar\omega$ calculation. In contrast, the inclusion of $2\hbar\omega$ configurations worsens the theoretical description of the relatively weak 5.920 MeV transition, and neither calculation explains the 4.774 MeV form factor. As noted above, most of the $C2$ strength is found in the 6.025 MeV transition and for this, while the $2\hbar\omega$ calculation provides some improvement over the $1p$-shell prediction, the theory still underestimates the data by more than a factor of 2.

In the previous section it was shown how a $2\hbar\omega$ shell model with Woods-Saxon radial wave functions can provide a satisfying fit to the elastic charge form factor. As

indicated in Fig. 8, this is not the case for the 6.025 MeV transition, where the predictions of the $2\hbar\omega$ model deteriorate when Woods-Saxon wave functions are used. The apparent agreement obtained for the elastic form factor may be a fortuitous result of the inability to separate the overlapping $C0$ and $C2$ multipole contributions.

A measure of the overall disagreement may be obtained by comparing the total experimental and theoretical form factors of the six levels included in Fig. 8. When the form factors are summed at their maxima it is found that the $2\hbar\omega$ model accounts for only 55% of the observed $C2$ strength, and the $1p$-shell model for 45%. As can be seen from the Appendix, similar results were obtained by extrapolating the (e,e') form factors to the low-q "photon point" limit $q = E_x$. Such a discrepancy [41] is also observed for the strong $[B(E2\uparrow) = 38.85 \pm 0.06 e^2\,\mathrm{fm}^4]$ quadrupole transition to the 4.439 MeV level in ^{12}C. These comparisons clearly show the need to consider configurations beyond the $2\hbar\omega$ model space. In particular, the extent of the discrepancy cannot be explained merely by using different radial wave functions.

In Fig. 9 the experimental results are compared to the first-order core-polarization calculations which include configurations up to $6\hbar\omega$ above the p shell. These calculations also use oscillator wave functions but with b=1.50 fm, as preferred for inelastic transitions by the authors of Ref. [7]. As will become clear, the adaptability in our choice of the oscillator size arises from the observation that there exists no unique value that best serves all form factors discussed here. The effect on longitudinal form factors of using the b=1.50 fm rather than b=1.70 fm is mainly to displace the form factor to larger q, with an 8% decrease in magnitude.

A more significant difference is that, unlike the (8-16)2BME p-shell results shown in Fig. 8, the core-polarization calculations presented in Fig. 9 are based on the Cohen-Kurath (8-16)POT and Hauge-Maripuu matrix elements. From these various results the sensitivity of the calculations to the assumed $1p$-shell interaction may be seen. For the J^π=1^+ and 2^+ states, the difference between the magnitudes of longitudinal form factors calculated using the (8-16)POT and (8-16)2BME matrix elements is generally $< 25\%$, although it amounts to a factor of 2 for the relatively weak 5.920 MeV transition. Much larger differences are found when the Cohen-Kurath results are compared to the Hauge-Maripuu predictions, particularly with regard to the 1^+ states at 0.718 and 2.154 MeV. The properties of these two states are known to be sensitive to configuration mixing, and the Hauge-Maripuu interaction clearly fails to get this right. On the other hand, for the strongly excited 4^+ state at 6.025 MeV the differences between the various calculations amount to only a few percent. The agreement in this case is not simply due to the large strength of the transition, but also to the relatively large J of the 6.025 MeV state; there are few nearby 4^+ states with which it can mix.

As indicated in Fig. 9, irrespective of the $1p$-shell model all calculated longitudinal form factors are markedly increased by core polarization. With one exception, the increase is by at least a factor of 1.8 at the maximum. These enhancements are relatively uniform over a large range in q; in particular, there are only small additional contributions from the $C4$ and higher multipoles disallowed by models confined to the $1p$ shell. The exception is the Hauge-Maripuu calculation for 0.718 MeV transition, where the 30% increase from core polarization is much too small to compensate for the inadequate $1p$-shell description. Especially for the 6.025 MeV level, which has almost 90% of the total $C2$ strength, the inclusion of core polarization brings the theoretical predictions into near quantitative agreement with the experimental results. Apart from this transition, the sensitivity of the theoretical predictions to the assumed $1p$-shell interaction restricts the usefulness of a level-to-level comparison of the core-polarization calculations and experimental results. As above, perhaps the most meaningful measure is the comparison of strengths obtained by summing the maximum values of the form factors, and when this is done the core-polarization calculations are found to account for roughly 90% of the experimental strength. The difference between the summed Cohen-Kurath and Hauge-Maripuu results is only a few percent. Core polarization is obviously essential for a quantitative understanding of the $C2$ transition strength.

2. *Transverse form factors*

Transverse components of these form factors are presented in Figs. 10 and 11. Unlike longitudinal excitations, where one multipole, $C2$, is always dominant, the $2\hbar\omega$ shell-model results indicate that $M1$, $E2$, and $M3$ multipoles can all make important contributions to transverse form factors. Compared to their longitudinal counterparts, the magnitudes of the calculated transverse form factors are somewhat more sensitive to the value of the oscillator size b. For example, when b is changed from 1.7

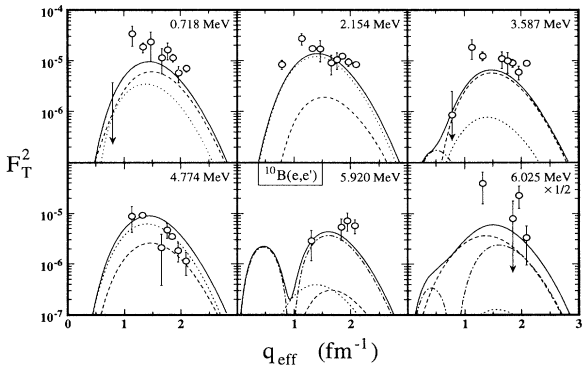

FIG. 10. Transverse form factors for transitions to even-parity states in ^{10}B. All experimental points are from the present experiment. Results of $2\hbar\omega$ shell-model calculations for the $M1$, $E2$, and $M3$ multipole contributions are indicated by the dot-dashed, dashed, and dotted curves, respectively. Solid curves show the sum of all possible multipole contributions. Oscillator wave functions were used with b=1.7 fm and for the 6.025 MeV transition both the data and the calculations have been multiplied by 1/2.

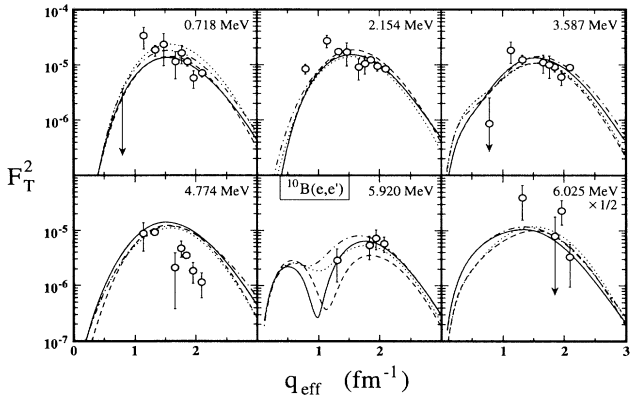

FIG. 11. Comparison of transverse form factors to the results of core-polarization calculations. The curves are identified according to the convention used in Fig. 9.

to 1.5 fm in $1p$-shell calculations, the maxima of transverse $E2$ and $M3$ form factors are increased by about 15%. Taking this into account, the difference between $1p$-shell calculations using the (8-16)2BME, (8-16)POT, and Hauge-Maripuu interactions is much less than a factor of 2 except for the 5.920 MeV (8-16)POT result. Again with this exception, for b=1.50 fm all p-shell calculations are in reasonable agreement with the data. Most remarkable is the comprehensive agreement obtained with the Hauge-Maripuu predictions that are so poor for the 0.718 and 2.154 MeV longitudinal form factors.

The result of including $2\hbar\omega$ configurations in the shell model is typically to reduce the $1p$-shell transverse calculation by a small amount. The effect of core polarization is even less; in some cases the $1p$-shell prediction is increased, while elsewhere it is decreased. As may be observed from Fig. 11, there is an apparent dependence on the $1p$-shell interaction model. For example, the (8-16)POT prediction for the transverse form factor of the 2.154 MeV excitation is decreased by 17% when core polarization is taken into account, whereas the corresponding Hauge-Maripuu prediction is increased by 8%.

Overall, the theoretical predictions for the transverse form factors are in unusually good agreement with the experimental results. In particular, there is little evidence of the systematic quenching seen in the transverse form factors of other $1p$-shell nuclei, most notably for the carbon isotopes [42–46]. Especially apparent in ^{10}B is the small dependence on the assumed $1p$-shell model, and relatively minor effects due to the inclusion of either $2\hbar\omega$ configurations or core polarization.

Finally, note should be made of the discrepant preferences of the longitudinal and transverse form factors for the value of the oscillator size parameter. Whereas the transverse form factors favor b=1.5 fm, the corresponding longitudinal form factors are best fit by values near 1.7 fm. As noted elsewhere [7], this may be the result of inappropriate choices made in our treatment of the core polarization which most strongly affects the longitudinal form factors. Indeed, Horikawa *et al.* [47] have emphasized that the results of $C2$ core-polarization calculations are quite dependent on the effective interaction. In their interpretation of $C2$ form factors in ^{15}N, Horikawa *et al.* [47] favored core polarization that decreases with increasing q. Expressed alternatively, their results suggested that the $C2$ "effective charge" associated with the core polarization should decrease at large q. Although the $C2$ effective charges deduced from our calculations also diminish with increasing q, they do so at a relatively slow rate, typically by $< 10\%$ between $q \approx 0$ and q=3 fm^{-1}. If the calculated core polarization were to decrease more quickly, the longitudinal form factors would be better fit by a smaller value of b, thus tending to bring the longitudinal and transverse form factors closer to consistency.

C. 4.774 MeV transition

The radiative decay of the J^π=3$^+$, T=0 state at 4.774 MeV to the ^{10}B ground state has long been known [48] to be retarded. Indeed, the explanation of the especially small $M1$ width constituted an early notable success of the p-shell models of Cohen and Kurath [21].

In Figs. 8 and 9 the sizable longitudinal form factor observed for the 4.774 MeV excitation is compared to the theoretical predictions, all of which are dominated by the C2 multipole. None of these calculations account for the observed form factor shape, which, compared to other $C2$ form factors, is displaced to low q. The comparisons are especially difficult at the photon point where most calculations give reduced transition probabilities $B(E2\uparrow)$ of 0.4–0.6e^2 fm^4, values that are at least 10 times the small upper limit of 0.04e^2 fm^4 deduced from the observed ground-state radiative width [13,49]. With a $B(E2\uparrow)$ value of 0.068e^2 fm^4, only the Hauge-Maripuu $1p$-shell calculation approaches the experimental result, but this model fails to explain the (e,e') form factor. Since there is little reason to doubt the smallness of the $E2$ width, one is led to consider the possibility of an interference effect in the form factor, one which would have to be almost completely destructive at very low q, but still leave substantial $C2$ strength in a broad region around q = 1fm^{-1}. We discount the likelihood of such pathological interference because it would likely introduce a diffraction minimum into the form factor at low q, a feature for which the data provide no evidence.

Of course, the J^π = 3$^+$ state may also be excited by $C0$, $C4$, and $C6$ multipoles; however, our calculations show that these contributions should be at least 2 orders-of-magnitude lower than the data near q = 1 fm^{-1}. Nevertheless, it is difficult to make realistic theoretical evaluations for $C0$ form factors since these depend sensitively on the radial shapes of single-particle wave functions, as well as admixtures of higher excited states [45]. As demonstrated in Fig. 9, the q dependence of the data is almost identical to the shape of the $C0$ form factor [45] observed for the 8.86 MeV transition in ^{13}C. Additional support for a $C0$ assignment comes from a fit [45] to the data which gives a value of 0.46 fm^{-2} for the monopole matrix element. This is comparable to monopole matrix elements deduced [45] for low-lying states in ^{13}C and ^{16}O. In the vicinity of q = 2 fm^{-1} the ^{10}B data are slightly larger than the $C0$ curve, however this excess strength is consistent with our core polarization calculations for the $C4$ multipole.

The monopole contribution vanishes for the transverse form factor of the 4.774 MeV form factor, which, as shown in Fig. 10, is in good agreement with the predicted dominant $M3$ component. This observation confirms the interpretation of (p,p') measurements by Lewis *et al.* [3].

D. Inelastic transitions to odd-parity states

Figure 12 shows the separated longitudinal and transverse form factors deduced for transitions to the odd-parity T=0 levels at 5.110, 6.127, and 6.561 MeV. No previous data exist for these excitations. The respective spin assignments for the first two levels are J=2$^-$ and 3$^-$; the 6.561 MeV level bears a tentative J=(4)$^-$ assignment. Also shown are the results of $1\hbar\omega$ shell-model calculations using a value of b=1.70 fm for the oscillator size. According to these predictions, the $C3$ multipole makes the largest contribution to the 6.127 and 6.561 MeV form factors, whereas $C1$ is most important for the 5.110 MeV transition. These longitudinal predictions are in moderate agreement with the data, although a larger value of b would displace the curves to lower q, thereby reducing the observed differences. Of particular note is the excellent theoretical description provided for the spectroscopic quantities and form factor of the 6.561 MeV level. These support the J=4$^-$, T=0 assignment for this state. As can be seen, although the experimental information on the transverse form factors is of rather meager statistical quality, the results are nonetheless consistent with the shell-model predictions.

E. $M3$, ΔT=1 transitions

The transverse form factors of the $M3$ transitions to the two T=1 levels at 1.740 and 5.163 MeV are much larger than the $E2$ form factors shown in Figs. 10 and 11. This is due to the large magnitude of the isovector (ΔT=1) magnetic moment $\mu_1 = (\mu_\pi - \mu_\nu)/2 = 2.353\mu_N$ in comparison to the isoscalar ($\Delta T = 0$) moment $\mu_0 = (\mu_\nu + \mu_\pi)/2 = 0.440\mu_N$. Another consequence of the isovector nature of these transitions is that the relative meson exchange contribution is larger, and hence this should be considered in theoretical evaluations.

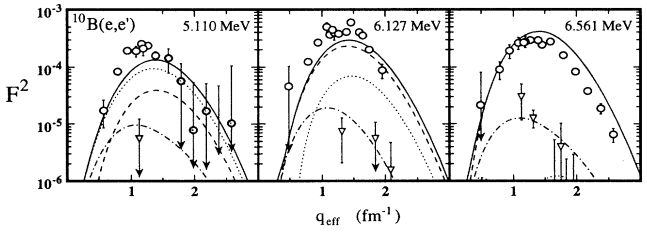

FIG. 12. Form factors obtained for transitions to odd-parity states in ^{10}B. All experimental results are from the present experiment, with the circles and triangles indicating the longitudinal and transverse form factors. The shaded points for the 5.110 MeV transition were derived from measurements which did not resolve this level from the nearby 5.164 MeV state, for which longitudinal excitation appears to be relatively weak. Results of $2\hbar\omega$ shell-model calculations for the $C1$ and $C3$ multipole contributions are, respectively, indicated by the dotted and dashed curves, whereas the solid curves are the sum of all possible longitudinal multipoles. Dot-dashed curves show the predicted total transverse form factor.

1. *Form factor for the 1.740 MeV transition and the $1p_{3/2}$ radial wave function*

As indicated by Fig. 13, the determination of the $M3$ 1.740 MeV form factor at $q < 2$ fm^{-1} is considerably improved by the new data. All data in this figure have been corrected for Coulomb distortion by means of an iterative procedure [50]. The curves result from shell-model calculations based on the (8-16)2BME 1p-shell amplitudes of Cohen and Kurath [21] and radial wave functions derived from a Woods-Saxon potential well. The inclusion of one-pion-exchange contributions [2] increases the magnitude of the form factor by 15% at the maximum, while having only a slight effect on the form-factor shape. Irrespective of whether meson exchange is considered or not, both curves lie in good quantitative agreement with the data, suggesting that the transition is reliably represented as the spin-flip transition of a $1p_{3/2}$ nucleon.

In accord with 1p-shell models, the data can be transformed to obtain the $1p_{3/2}$ wave function [2], provided that a correction is first made for meson-exchange contributions. Following subtraction of the calculated one-pion exchange component, a Fourier-Bessel analysis [51] led to the wave-function error band shown in Fig. 14. The cutoff radius for this analysis was 7.5 fm; smearing of the wave function due to the finite nucleon size was factored

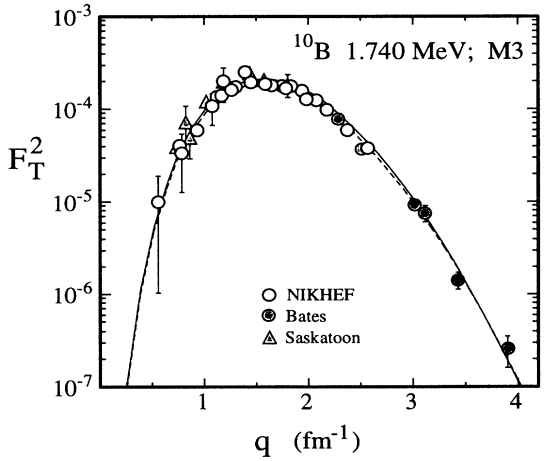

FIG. 13. $M3$ form factor for the 1.740 MeV transition in ^{10}B. The data, corrected for Coulomb distortion, are from the present experiment (open circles), Hicks *et al.* [2] (solid circles), and Ansaldo *et al.* [6] (triangles). The curves represent theoretical calculations using the (8-16)2BME 1p-shell amplitudes [21] and Woods-Saxon radial wave functions. The solid curve includes one-pion-exchange contributions; the dashed curve does not.

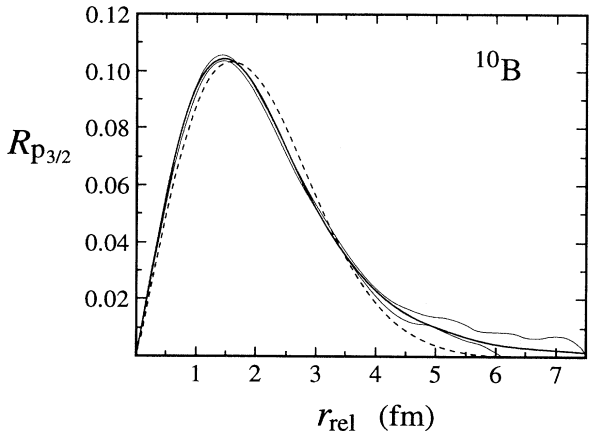

FIG. 14. $1p_{3/2}$ wave function obtained by transforming form-factor data for the 1.740 MeV $M3$ transition, shown as a function of the relative core-particle separation. Calculated one-pion-exchange contributions were first subtracted from the data. The shaded error band shows the result of a Fourier-Bessel analysis. Solid and dashed curves represent the Woods-Saxon and harmonic-oscillator wave functions that best fit the data.

out. In order to damp out unphysical oscillations in the fitted wave function at large r the fit was weakly biased [51] to approximate a Woods-Saxon dependence beyond r=4.5 fm. Compared to our earlier result [2], the width of the error band is reduced by about a factor of 2 for $r > 3$ fm.

Also shown in Fig. 14 are the wave functions corresponding to harmonic-oscillator and Woods-Saxon fits to the data. The experimental results are poorly fit by oscillator wave functions, which decrease too quickly at large r. Much more satisfactory is a two-parameter Woods-Saxon fit, in which the free parameters were the radius and diffuseness of the potential well. The total χ^2 obtained in this analysis, 49.3 for 39 data points, was almost as small as that given by the eight-parameter Fourier-Bessel fit. For simplicity, the Woods-Saxon spin-orbit force was neglected and the $1p_{3/2}$ binding energy was set to 7.0 MeV, a value close to the observed neutron and proton separation energies for ^{10}B.

In the relative core-particle coordinate frame [37] the best-fit Woods-Saxon parameters were $R = (0.88 \pm 0.13)$ $(A-1)^{1/3}$ fm for the well radius and $z = 0.81 \pm 0.08$ fm for the diffuseness. The corresponding rms radius of the $1p_{3/2}$ orbit is 2.79 ± 0.02 fm, with the smallness of the error reflecting the correlation between R and z. For the Fourier-Bessel fit the deduced rms radius is 2.79±0.11 fm. The much larger error given by the Fourier-Bessel analysis is due to the shape of the wave function at large r being relatively unconstrained compared to the Woods-Saxon description. This result serves as a caution for previous determinations of valence orbital sizes in odd-A nuclei from elastic magnetic (e,e') form factors. Because of the superimposed contributions of lower-order magnetic multipoles at $q \leq 2$ fm^{-1}, these orbital sizes are obtained from just the high-q part of data belonging to the largest ΔJ multipole. Very precise values for orbital sizes have been published [1]; however, these rely upon specific model assumptions, usually a Woods-Saxon dependence, for the r dependence of the radial wave functions. Only in the present case may the entire q range of the form factor be exploited to determine the orbital size. As has been demonstrated, the absence of overlapping multipoles makes it possible to determine not just the size but the full r dependence of the wave function throughout the nuclear interior.

Despite this positive conclusion, the assumptions underlying the present analysis merit critical examination. For example, because both proton and neutron excitation contribute to the pure isovector $M3$ transition, Eq. (1) can be expressed in the more general form

$$F_{M3}(q) \propto q\mu_\pi \int_0^\infty |\, R^\pi_{p_{3/2}}(r)\,|^2\, j_2(qr) r^2 dr - q\mu_\nu \int_0^\infty |\, R^\nu_{p_{3/2}}(r)\,|^2\, j_2(qr) r^2 dr\ ,$$

where $\mu_\pi = 2.793\mu_N$ and $\mu_\nu = -1.913\mu_N$ are the proton and neutron magnetic moments. The form factor is therefore seen to be more sensitive to the proton distribution. Differences between the single-particle wave functions $R^\pi_{p_{3/2}}(r)$ and $R^\nu_{p_{3/2}}(r)$ arise from the Coulomb barrier. Nevertheless, these are relatively small for the Z=4 core of ^{10}B. Calculations in otherwise identical Woods-Saxon wells give a difference of about 2% between the sizes of the proton and neutron orbits. For self-conjugate ^{10}B there is no experimental evidence to suggest that proton and neutron distributions should be significantly different.

Contributions to the form factor from meson-exchange currents were evaluated using the shell-model amplitudes of Cohen and Kurath [21] and harmonic-oscillator wave functions. The oscillator size parameter was b=1.55 fm, a value close to optimum for an oscillator fit to the $M3$ form factor. As indicated above, for this form factor the meson-exchange contribution has almost the same q dependence as the one-body part. Hence the effect of the meson-exchange correction on the deduced wave function is relatively small: Inclusion of this correction increases the deduced rms size by 1.7%.

Admixtures in the ^{10}B wave functions of higher-excited orbits would also affect the interpretation. The effect of such admixtures was previously investigated [2] by performing additional shell-model calculations in a complete $2\hbar\omega$ basis space. When the data were corrected for these admixtures, the deduced rms size was smaller by $\leq 2\%$. Thus, according to these calculations, the corrections to the rms size from meson-exchange and higher-order shell-model components are both $\leq 2\%$, each barely half the uncertainty stemming from the imprecisely determined shape of the wave function at $r > 4$. Moreover, the two corrections tend to cancel.

To what extent can core polarization affect the conclusions? The results presented thus far give no conclusive evidence for sizable core-polarization contributions to *transverse* form factors. As may be observed from Fig. 11, for example, the inclusion of core polarization changes the magnitude of the $1p$-shell predictions for these form factors by typically $< 25\%$, sometimes as

an increase, but just as likely as a decrease, depending on the p-shell interaction model. The precision of the experimental results presented in Fig. 11 is insufficient to indicate a clear preference for any particular calculation, with or without core polarization. Moreover, as previously reported [2], and further confirmed by Fig. 13, the magnetic form factors of boron isotopes are quantitatively well described by $1p$-shell computations that use Woods-Saxon radial wave functions.

Nevertheless, calculations [7] specifically for the 1.740 MeV transition in ^{10}B suggest that the effects of core polarization cannot be neglected, especially if precise information is sought on the radial distribution of the valence orbit. This is seen, for example, in Fig. 15 which shows modifications to the form factor due to core polarization and meson exchange on a calculation that used oscillator radial wave functions and (8-16)POT $1p$-shell matrix elements. At the maximum of the $M3$ form factor meson exchange increases the $1p$-shell predictions by about 15%. (As previously noted, this enhancement was accounted for in the extraction from the data of the $1p_{3/2}$ radial wave function.) However, the effect of isovector core polarization is calculated to be unexpectedly large for a transverse form factor: At the maximum of the $M3$ form factor core polarization interferes destructively with the p-shell and meson-exchange components, *reducing* the theoretical prediction by about 35%. Furthermore, core polarization is predicted to modify the form factor in a way that is q dependent: At q=3.9 fm^{-1}, the highest momentum transfer point available from experiment, core polarization *increases* the calculation by a factor of approximately 5. Almost the same effects are obtained when the calculations are repeated with the Hauge-Maripuu potential. In contradiction then to the Woods-Saxon results presented in Fig. 13, Fig. 15 indicates that good agreement cannot be obtained with the data unless core polarization is specifically included.

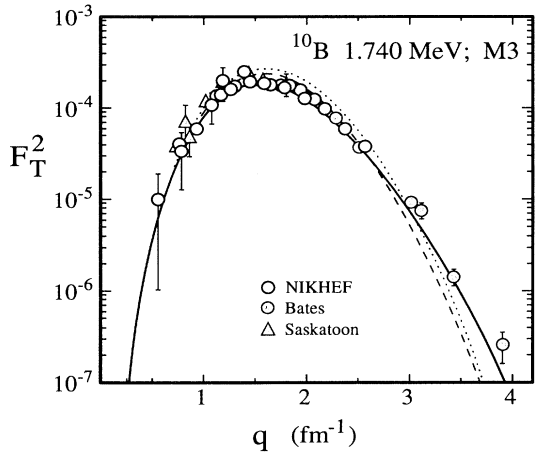

FIG. 15. $M3$ form factor obtained for the 1.740 MeV transition in ^{10}B, as in Fig. 13. Theoretical curves were obtained using oscillator wave functions (b=1.50 fm) and the (8-16)POT interaction. Dashed curve, $1p$-shell contributions only; dotted curve, $1p$-shell plus meson exchange currents; solid curve, sum of $1p$-shell, meson-exchange current, and core-polarization contributions.

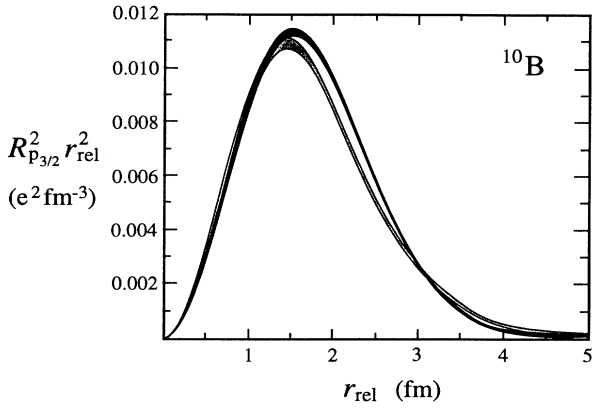

FIG. 16. $1p_{3/2}$ radial densities obtained by transforming data for the 1.740 MeV $M3$ transition. The lightly shaded error band corresponds to the Fourier-Bessel result shown in Fig. 14; the solid band is the result of an analysis in which calculated core-polarization and meson-exchange contributions were first subtracted from the data.

Figure 16 illustrates the extent to which core polarization may modify the extracted $1p_{3/2}$ radial density. Both error bands were obtained by transforming form-factor data from which calculated exchange-current contributions had first been removed. Predicted core-polarization parts have also been subtracted in one case, the effect of which is to displace the maximum of the density to a larger radius. The density obtained in this way then decreases more quickly with increasing r, with the result that the rms radius is reduced by 5%. In light of the results presented in Fig. 15, it is not surprising that the modified density is more compatible with a harmonic-oscillator dependence, although a Woods-Saxon fit with a small diffuseness value, z=0.31 fm, is still superior.

2. 5.164 MeV M3 transition

Except at low momentum transfer, the (e, e') form factor for the transition to the 5.164 MeV J^π=2$^+$, T=1 state is also dominated by the $M3$ multipole. Unlike previous measurements, most of our spectra had sufficient resolution to resolve this state from nearby T=0 states at 5.110 MeV (J^π=2$^-$) and 5.18 MeV (J^π=1$^+$). No evidence was found for the excitation of the broad ($\Gamma \approx$ 110 keV) level at 5.18 MeV, and the 5.110 MeV excitation was apparent only through its appreciable longitudinal form factor; the transverse strength of the triplet belongs almost entirely to the 5.164 MeV transition.

As previously noted [2], the shape of the transverse form factor for the 5.164 MeV transition is close to that of the 1.740 MeV $M3$ transition. In Fig. 17 this form factor is compared to the results of two shell-model calculations, both of which utilized Woods-Saxon wave functions. Because of the dominance of the $M3$ component, it is reasonable to utilize the Woods-Saxon potential parameters obtained from the fit to the 1.740 MeV form factor. As indicated by the figure, the calculation based on the (8-16)2BME $1p$-shell amplitudes provides an approximate

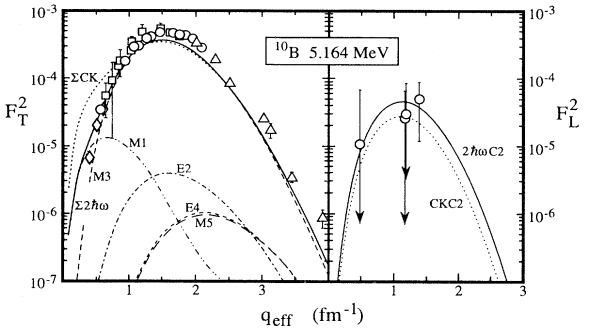

FIG. 17. Form factors for the transition to the 5.164 MeV $J^\pi=2^+$ state in ^{10}B. Results from the present experiment are indicated by circles; previously published data are from Fagg *et al.* [10] (lozenges), Ansaldo *et al.* [6] (squares), and Hicks *et al.* [2] (triangles). For the shaded points the 5.164 MeV level was not resolved from the nearby 5.110 MeV $J^\pi = 2^-$ level. The curves are shell-model results using Woods-Saxon radial wave functions for the transverse form factors, and harmonic-oscillator wave functions (b=1.70 fm) for the longitudinal. The dotted curves were derived from the (8-16)2BME $1p$-shell amplitudes, with the ΣCK result representing the total transverse form factor. All other curves result from a $2\hbar\omega$ shell-model calculation. Meson-exchange contributions are not included.

description of the data, although the $M1$ component is too large. This defect is largely remedied by the $2\hbar\omega$ shell-model calculation. Note that, even in this model, the contributions of the $E2$, $E4$, and $M5$ multipoles are negligible.

For comparison, Fig. 18 shows the results of oscillator calculations based on the (8-16)POT and Hauge-Maripuu amplitudes. Although not directly indicated by the figure, there is some sensitivity to the $1p$-shell interaction:

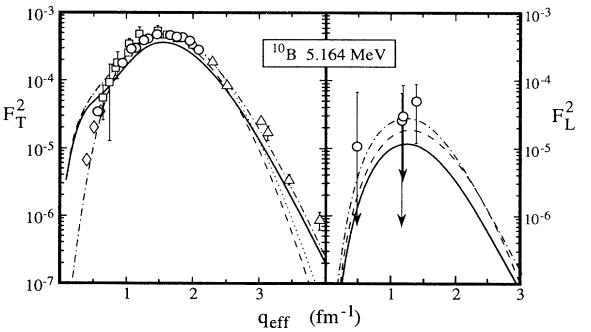

FIG. 18. Form factors for the transition to the 5.164 MeV level. The experimental data are as indicated in Fig. 17 and the curves result from shell-model calculations using oscillator radial wave functions with b=1.50 fm. Dashed curves, $1p$-shell calculation with (8-16)POT amplitudes; dotted curves, $1p$-shell plus exchange currents; solid curves, sum of $1p$-shell, exchange-current, and core-polarization contributions. The dot-dashed curves show form factors obtained with the Hauge-Maripuu interaction. The very small meson-exchange contributions were not calculated for the longitudinal form factor.

At the maximum the Hauge-Maripuu form factor is 55% larger than the (8-16)POT prediction. Nevertheless, the main intent of Fig. 18 is to indicate the size of the calculated core-polarization and transverse exchange-current contributions. The results are similar to those obtained for the 1.740 MeV $M3$ transition: At the maximum, the transverse form factor is raised by 14% as a result of exchange currents, but decreased by about 30% by core polarization. Again, the q dependence of the core-polarization contribution modifies the calculation in an essential way, boosting the form factor at high momentum transfer to overcome a too rapid falloff in the $1p$-shell part. These effects are rather independent of the assumed $1p$-shell interaction.

As with the (8-16)2BME potential, the (8-16)POT potential gives an $M1$ component that is too large, a problem that is unresolved by core polarization. For this form factor the Hauge-Maripuu interaction is more successful, explaining the small $M1$ form factor as the result of destructive interference between spin-flip and convection currents, an interpretation favored by photopion measurements [7,52].

Also shown in Figs. 17 and 18 are results for the longitudinal part of the 5.164 MeV transition. Although the data lack precision, they are nevertheless comparable in magnitude to the various shell-model predictions.

V. SUMMARY AND CONCLUSIONS

We have presented the first comprehensive, good-resolution measurements of electron scattering from low-lying levels of ^{10}B. With the exception of the broad 5.18 MeV level, form factors were obtained for all levels up to 6.7 MeV.

Although the statistical quality of our results for the longitudinal elastic form factor is much superior to those from the only prior experiment [12], the model dependence of separating the $C0$ and $C2$ components still prevents the ground-state charge density from being precisely determined. For the three-parameter Fermi representation of the density the following values were obtained: c=2.01 ± 0.33 fm, z=0.55 ± 0.06 fm, and w=0.0 ± 0.7, corresponding to an rms radius of 2.58 ± 0.05 ± 0.05 fm. The increase in the rms size over the 2.45 ± 0.12 fm resulting from the harmonic-oscillator analysis of Stovall *et al.* [12] arises from our use of a more realistic nuclear density model.

The new result for the rms size is just barely consistent with the value of 2.44 ± 0.06 fm deduced by Olin *et al.* [33] from measurements of muonic x-ray energy shifts. Muonic x-ray experiments yield only a moment of the ground-state charge distribution, not the detailed information on the radial charge distribution that can be derived from electron scattering *provided that the C0 form factor is unambiguously determined.* Although not possible in our experiment, the $C0$ component could be isolated in an electron-scattering measurement using a polarized beam and polarized target, experimental capabilities currently under development.

The two isovector form factors measured in this work,

for the 1.740 and 5.164 MeV transitions, are characterized by dominant transverse $M3$ multipoles. In contrast, isoscalar transitions were observed mainly through their longitudinal form factors: All isoscalar transitions to natural-parity states have dominant $C2$ multipoles, whereas the $C1$ and $C3$ multipoles were most important for the isoscalar, parity-changing transitions.

The availability of these diverse results provides comprehensive tests of nuclear models for ^{10}B. Examined in this work were conventional $1p$-shell models, models with $1\hbar\omega$ and $2\hbar\omega$ configurations in the $1s$, $2s1d$, and $2p1f$ shells, and finally, the extension of the shell model by core polarization.

The restricted $1p$-shell models are quite successful in describing properties such as the ^{10}B level spectrum and transverse form factors. Less satisfactory are the $1p$-shell predictions for the $C2$ form factors: Not only is there considerable dependence on the $1p$-shell interaction, but these models give just 45% of the total observed $C2$ transition strength. Only a 10% improvement was realized by expanding the shell-model space to include $2\hbar\omega$ configurations. The inclusion of even higher-excited configurations proved essential in order to resolve the shortfall. When this was done, by means of a core-polarization calculation, approximately 90% of the $C2$ strength was accounted for. On the other hand, it was found that comparisons based on isolated levels can be misleading: Even full core-polarization results are often in substantial disagreement with the data. In part, this is due to the underlying sensitivity to the assumed $1p$-shell interaction. No particular p-shell interaction was found to give a consistently satisfactory description for all levels. However, the Cohen and Kurath interactions may be preferable because the Hauge-Maripuu predictions are in marked disagreement with the longitudinal results for the $J=1^+$ states at 0.718 and 2.154 MeV.

The conclusions drawn from the transverse form factors are strikingly different. In this case all $1p$-shell interactions are consistent with the experimental results. For example, even for the two $J=1^+$ states, transverse form factors calculated using Hauge-Maripuu matrix elements are in excellent agreement with the data.

Conflicting conclusions may be reached regarding the importance of $2\hbar\omega$ configurations and core polarization for transverse form factors. The largest $2\hbar\omega$ effects on transverse form factors were found for multipoles that were weak in $1p$-shell calculations, for example, the $M3$ elastic form factor and the $M1$ component of the 5.164 MeV transition. Otherwise, the predicted effects are small, typically $< 10\%$, and quite undistinctive. The largest effect of core polarization is predicted for the isovector $M3$ form factors, a result that hinders a model-independent determination of the $1p_{3/2}$ radial density, one of the main goals of this investigation. It has been shown how a core-polarization calculation with oscillator wave functions *reduces* a $1p$-shell calculation by about 35% at the maximum of the $M3$ form factor. However, the interference is q dependent, so that near $q=4$ fm^{-1}, the highest momentum transfer probed, the $1p$-shell result is *increased* by a factor of 5. The overall effect of these modifications is to correct deficiencies in the $1p$-shell oscillator calculation and give a fit to the experimental results that is entirely satisfactory. From this analysis it appears that a sizable core polarization contribution is essential in order to understand the $M3$ form factors of ^{10}B.

A contradictory interpretation comes from a previous paper [2], where we demonstrated how magnetic form factors for four levels in ^{10}B and ^{11}B can be well understood on the basis of $1p$-shell amplitudes and meson-exchange currents, without any apparent need for core polarization, provided Woods-Saxon radial wave functions are used. In comparison to harmonic-oscillator results, the use of Woods-Saxon wave functions reduces the magnitude of calculated magnetic form factors near $q=1.5$ fm^{-1}, but increases the form factors at high $q \gtrsim 3$ fm^{-1}, a result quantitatively similar to the effect of core polarization on the oscillator calculation.

Thus the importance of core polarization in transverse form factors remains an open question. Comprehensive measurements, such as those presented here, provide opportunities for systematic theoretical investigations of the interference between the leading-order shell-model terms and core-polarization collectivity. Of particular value may be transitions such as the $C0$ 4.774 MeV excitation, where configurations involving particles outside the $1p$ shell appear to make especially strong contributions.

The ^{12}C and ^{13}C nuclei provide additional opportunities for testing core-polarization concepts [31,44]. In particular, $1p$-shell models can explain measurements of $M4$ form factors that extend beyond $q=4$ fm^{-1}. One interpretation [53] of the apparently small core-polarization contributions to higher multipole magnetic form factors is that, because of the relatively large angular momentum transfer, one-body electromagnetic transitions are confined to the single-particle levels in each shell that have the largest j. This restriction reduces possibilities for configuration mixing, leaving the lowest-energy configurations to dominate. On this basis, the $M3$ form factor may be argued to be reliably represented as a $1p_{3/2} \rightarrow 1p_{3/2}$ transition. Although this notion is confirmed by Woods-Saxon calculations, core-polarization calculations suggest otherwise.

The ambiguities discussed above in no way detract from the remarkable success of the shell model for $1p$-shell nuclei. Interactions proposed three decades ago by Cohen and Kurath and others provide, for the most part, compellingly sound predictions of the energies of low-lying natural-parity states, magnetic moments, and transition rates, as well as scattering and reaction cross sections. As more experimental results have become progressively available the success of these interaction models grows even more noteworthy. It is the improvement beyond these $1p$-shell models that has proved so challenging.

Considerable attention has been given to the core-polarization predictions for ^{10}B. Despite the encouraging success of this formalism with regard to the longitudinal $C2$ form factors, for example, several uncertainties remain unresolved. A potential inadequacy is indicated by the failure, even when core polarization is included, to find a unique potential size parameter that gives a

consistent account of all form factors measured in ^{10}B. Moreover, oscillator wave functions are of doubtful reliability for calculating form factors that span a large range in q, suggesting that the oscillator model may not be the most appropriate choice for the basis wave functions in core-polarization treatments.

A further concern is that if first-order core polarization is important, then why not higher-order core polarization involving more than one particle or hole outside the valence shell? For example, in their evaluations of the magnetic elastic form factors of ^{15}N and ^{17}O, Blunden and Castel [54] and Gökalp and Yilmaz [55] found that the effect of second-order core polarization was comparable to that of first order, with both corrections giving reductions relative to the $1p$-shell calculation. In the case of ^{15}N, the second-order correction impaired the agreement with the experimental results.

Subject to basis-space limitations, such configurations can also be calculated using multi-$\hbar\omega$ shell models. According to our results for $C2$ form factors, it would appear that while the $2\hbar\omega$ shell model provides a useful enhancement over $1p$-shell predictions, the participation of $> 2\hbar\omega$ configurations is essential in order to achieve final agreement. Nevertheless, as with the $1p$-shell calculations, the multi-$\hbar\omega$ shell-model results have a non-negligible dependence on the assumed interaction. For example, calculations by Booten *et al.* [56] using a different shell-model interaction show that $C2$ form factors measured in ^{7}Li can be largely explained by $2\hbar\omega$ configurations. Furthermore, calculations by this group [57] give somewhat larger $2\hbar\omega$ effects for ^{10}B magnetic form factors than those reported here.

A final uncertainty, important for transverse isovector transitions, is the unknown accuracy of meson-exchange calculations. Only for A=2 and A=3 nuclei is there evidence [44] to support the reliability of meson-exchange treatments.

In conclusion, then, notwithstanding considerable theoretical effort, the merits of present $2\hbar\omega$, core-polarization, and meson-exchange models have yet to be fully established. Because the testing of these models is usually hindered by interpretational ambiguities, the most instructive insights may come from comparisons of experimental results from a variety of reactions that have different and complementary sensitivities to nuclear structure and reaction mechanisms [7,31,52].

ACKNOWLEDGMENTS

W. Lozowski and G. Hudson of the Indiana University Cyclotron Facility are thanked for their guidance and assistance with the construction of the ^{10}B targets. We are grateful to the NIKHEF accelerator staff, to the NIKHEF graduate students who assisted with the data-taking, and to Dr. J. Gallant for numerical computations. Special thanks are due to Dr. J. Millener and to Dr. D. Kurath for insights into the interpretation of the 4.774 MeV transition. This work was supported by the U.S. Department of Energy and belongs, in part, to the program of the Foundation for Fundamental Research of Matter (FOM), which is financed by the Netherlands' Organization for the Advancement of Pure Research (NWO).

APPENDIX: $B(E2\uparrow)$ VALUES

The reduced matrix element $B(E2\uparrow, E_x)$, or, equivalently, the ground-state radiative width, has also been utilized [8–10,21–24] as a point of comparison for ^{10}B results. This matrix element can be determined [14] by extrapolating the (e,e') form factor to the low-q "photon point" limit $q = E_x$:

$$B(E2\uparrow, E_x) = \lim_{q\to E_x} \frac{(15Z)^2}{4\pi} \frac{F_{C2}^2(q)}{q^4} \ . \tag{A1}$$

The model dependence of this procedure depends on how closely the available data approach the $q = E_x$ limit. As it was not an objective of the present experiment to obtain such spectroscopic information, our data are mainly confined to the region $q_{\rm eff} > 0.5$ fm^{-1}. Nevertheless, useful results were obtained by fitting the data with expressions having the form of Eq. (4). In Table II these results

TABLE II. Experimental and theoretical values of the reduced transition probabilities $B(E2\uparrow)$ (e^2 fm^4) for ^{10}B. The present experimental results are compared to values tabulated by Barker [24]. The theoretical values, for two different $1p$-shell interactions, differ according to the consideration or neglect of $2\hbar\omega$ configurations and core polarization (cp). All calculations used oscillator wave functions with b=1.6. Note that for these wave functions $B(E2\uparrow)\propto b^4$.

		Experiment		Theory				
				(8-16)2BME			(8-16)POT	
E_x (MeV)	J^π	Barker	Present	$1p$	$1p+2\hbar\omega$	$1p$ + cp	$1p$	$1p$ + cp
0.718	1^+	1.81 ± 0.03	1.7 ± 0.3	0.70	0.79	1.64	0.68	1.62
2.154	1^+	0.70 ± 0.08	0.4 ± 0.1	0.10	0.27	0.20	0.13	0.28
3.587	2^+	0.87 ± 0.25	0.6 ± 0.1	0.54	0.60	1.36	0.44	1.13
4.774	3^+	< 0.04		0.54	0.44	1.54	0.56	1.63
5.920	2^+	0.15 ± 0.03	0.17 ± 0.05	0.10	0.07	0.17	0.20	0.39
6.025	4^+	24.4 ± 3.9	17.4 ± 0.7	4.42	5.38	11.70	4.44	11.74
Total		27.9 ± 3.9	20.3 ± 0.8	6.40	7.55	16.6	6.45	16.8

are compared to theoretical values, as well as a prior tabulation of experimental results by Barker [24]. The two sets of experimental values are generally consistent, although we obtain a $B(E2\uparrow)$ value for the very strong 6.025 MeV excitation that is approximately 30% smaller than the result listed by Barker. This discrepancy was not anticipated since Barker's value is taken from a previous (e,e') measurement [9], the results of which were also included in our analysis. The larger values obtained in previous analyses [6,8,9] of this form factor are due to the neglect of Coulomb distortion effects. Although the nuclear charge is small, so were the incident beam energies in these measurements, as low as 32 MeV in the case of the Darmstadt measurement [9], and the effect on the reduced matrix element is appreciable.

[1] T. W. Donnelly and I. Sick, Rev. Mod. Phys. **56**, 461 (1984).
[2] R. S. Hicks, J. Button-Shafer, B. Debebe, J. Dubach, A. Hotta, R. L. Huffman, R. A. Lindgren, G. A. Peterson, R. P. Singhal, and C. W. de Jager, Phys. Rev. Lett. **60**, 905 (1988).
[3] P. R. Lewis, G. G. Shute, B. M. Spicer, R. S. Henderson, R. Abegg, D. Frekers, O. Häusser, K. P. Jackson, C. A. Miller, and S. Yen, Nucl. Phys. **A532**, 583 (1991).
[4] L. Wang, X. Yang, J. Rapaport, C. D. Goodman, C. C. Foster, Y. Wang, R. A. Lindgren, E. Sugarbaker, D. Marchlenski, S. de Lucia, B. Luther, L. Rybarcyk, T. N. Taddeucci, and B. K. Park, Phys. Rev. C **47**, 2123 (1993).
[5] H. Baghaei, R. A. Lindgren, P. Slocum, A. J. Stephenson, A. D. Bacher, S. Chang, J. Lisantti, J. Liu, C. Olmer, S. Wells, S. W. Wissink, B. L. Clausen, J. A. Carr, S. K. Yoon, and F. Petrovich, Phys. Rev. C **69**, 2054 (1992).
[6] E. J. Ansaldo, J. C. Bergstrom, R. Yen, and H. S. Caplan, Nucl. Phys. **A322**, 237 (1979).
[7] T. Sato, N. Odagawa, H. Ohtsubo, and T.-S. H. Lee, Phys. Rev. C **49**, 776 (1994).
[8] G. Fricke, G. R. Bishop, and D. B. Isabelle, Nucl. Phys. **67**, 187 (1965).
[9] E. Spamer, Z. Phys. **191**, 24 (1966).
[10] L. W. Fagg, R. A. Lindgren, W. L. Bendel, and E. C. Jones, Jr., Phys. Rev. C **14**, 1727 (1976).
[11] P. Kossanyi-Demay and G. J. Vanpraet, Nucl. Phys. **81**, 529 (1966).
[12] T. Stovall, J. Goldemberg, and D. B. Isabelle, Nucl. Phys. **86**, 225 (1966).
[13] D. E. Alburger, P. D. Parker, D. J. Bredin, D. H. Wilkinson, P. F. Donovan, A. Gallmann, R. E. Pixley, L. F. Chase, Jr., and R. E. McDonald, Phys. Rev. **143**, 692 (1966).
[14] H. Überall, *Electron Scattering from Complex Nuclei* (Academic, New York, 1971), Pt. B, Chap. 6.
[15] C. de Vries, C. W. de Jager, L. Lapikás, G. Luijckx, R. Maas, H. de Vries, and P. K. A. de Witt Huberts, Nucl. Instrum. Methods **223**, 1 (1984).
[16] Eagle Picher Industries, Inc., Miami, OK.
[17] J. W. de Vries, Ph.D. thesis, University of Utrecht, 1987; A. J. C. Burghardt, Ph.D. thesis, University of Amsterdam, 1988.
[18] E. A. J. M. Offerman, L. S. Cardman, C. W. de Jager, H. Miska, C. de Vries, and H. de Vries, Phys. Rev. C **44**, 1096 (1991).
[19] T. de Forest and J. D. Walecka, Adv. Phys. **15**, 1 (1966).
[20] D. R. Inglis, Rev. Mod. Phys. **25**, 390 (1953).
[21] S. Cohen and D. Kurath, Nucl. Phys. **73**, 1 (1965).
[22] E. K. Warburton, J. W. Olness, S. D. Bloom, and A. R. Poletti, Phys. Rev. **171**, 1178 (1968).
[23] D. Kurath, Nucl. Phys. **A317**, 175 (1979).
[24] F. C. Barker, Aust. J. Phys. **34**, 7 (1981).
[25] J. P. Elliot, A. D. Jackson, H. A. Mavromatis, E. A. Sanderson, and B. Singh, Nucl. Phys. **A121**, 241 (1968).
[26] P. S. Hauge and S. Maripuu, Phys. Rev. C **8**, 1609 (1973).
[27] D. J. Millener and D. Kurath, Nucl. Phys. **A255**, 315, (1975).
[28] A. G. M. van Hees and P. W. M. Glaudemans, Z. Phys. A **315**, 223 (1984).
[29] H. Nishioka, J. Phys. G **10**, 1713 (1985).
[30] G. Dearnaley, D. S. Gemmell, and S. S. Hanna, Nucl. Phys. **36**, 71 (1972).
[31] T. Sato, K. Koshigiri, and H. Ohtsubo, Z. Phys. A **320**, 507 (1985).
[32] G. Bertsch, J. Borysowicz, H. McManus, and W. G. Love, Nucl. Phys. **A284**, 399 (1977).
[33] A. Olin, P. R. Poffenberger, G. A. Beer, J. A. MacDonald, G. R. Mason, and R. M. Pearce, Nucl. Phys. **A360**, 426 (1981).
[34] R. K. Nesbet, Phys. Rev. A **2**, 1208 (1970).
[35] L. A. Schaller, L. Schellenberg, A. Ruetschi, and H. Schneuwly, Nucl. Phys. **A343**, 333 (1980).
[36] W. Ruckstuhl, B. Aas, W. Beer, I. Beltrami, K. Bos, P. F. A. Goudsmit, H. J. Leisi, G. Strassner, and A. Vachi, Nucl. Phys. **A430**, 685 (1984).
[37] D. J. Millener, J. W. Olness, E. K. Warburton, and S. S. Hanna, Phys. Rev. C **28**, 497 (1983).
[38] L. Lapikás, in *Modern Trends in Elastic Electron Scattering*, Proceedings of the First Miniconference, edited by C. de Vries (Nat. Inst. voor Kernfysica en Hoge-Energiefysica, Postbus 4395, 1009 AJ Amsterdam, The Netherlands, 1978), p. 49.
[39] R. E. Rand, R. Frosch, and M. R. Yearian, Phys. Rev. **144**, 859 (1966).
[40] H. G. Clerc and E. Kuphal, Z. Phys. **211**, 452 (1968).
[41] J. B. Flanz, R. S. Hicks, R. A. Lindgren, G. A. Peterson, A. Hotta, B. Parker, and R. C. York, Phys. Rev. Lett. **41**, 1642 (1978).
[42] R. S. Hicks, J. B. Flanz, R. A. Lindgren, G. A. Peterson, L. W. Fagg, and D. J. Millener, Phys. Rev. C **30**, 1 (1984).
[43] R. S. Hicks, in *Nuclear Structure in the 1p shell*, Proceedings of the Fourth Miniconference, edited by L. Lapikas, H. de Vries, and C. de Vries (Nat. Inst. voor Kernfysica en Hoge-Energiefysica, Postbus 4395, 1009 AJ Amsterdam, The Netherlands, 1985), p. 173.
[44] R. S. Hicks, R. L. Huffman, R. A. Lindgren, G. A. Peterson, M. A. Plum, and J. Button-Shafer, Phys. Rev. C **36**, 485 (1987).
[45] D. J. Millener, D. I. Sober, H. Crannell, J. T. O'Brien, L.

W. Fagg, S. Kowalski, C. F. Williamson, and L. Lapikás, Phys. Rev. C **39**, 14 (1989); D. J. Millener (private communications).

[46] M. A. Plum, R. A. Lindgren, J. Dubach, R. S. Hicks, R. L. Huffman, B. Parker, G. A. Peterson, J. Alster, J. Lichtenstadt, M. A. Moinester, and H. Baer, Phys. Rev. C **40**, 1861 (1989).

[47] Y. Horikawa, T. Hoshino, and A. Arima, Nucl. Phys. **278**, 297 (1977).

[48] D. H. Wilkinson and G. A. Jones, Phys. Rev. **91**, 1575 (1953).

[49] R. H. Spear, Z. E. Switkowski, D. L. Kennedy, and J. C. P. Heggie, Nucl. Phys. **318**, 21 (1979).

[50] U. Deutschmann, G. Lahm, R. Neuhausen, and J. C. Bergstrom, Nucl. Phys. **411**, 337 (1983).

[51] J. Heisenberg, in *Advances in Nuclear Physics*, edited by J. W. Negele and E. Vogt (Plenum, New York, 1981), Vol. 12, p. 61.

[52] T. Sato, N. Odagawa, H. Ohtsubo, and T.-S. H. Lee, Nucl. Phys. **A577**, 219c (1994).

[53] S. Raman, L. W. Fagg, and R. S. Hicks, in *Electric and Magnetic Giant Resonances in Nuclei*, edited by J. Speth (World Scientific, Singapore, 1991), p. 355.

[54] P. G. Blunden and B. Castel, Nucl. Phys. **A445**, 742 (1985).

[55] A. Gökalp and O. Yilmaz, Nuovo Cimento A **105**, 695 (1992).

[56] J. G. L. Booten, A. G. M. van Hees, P. W. M. Glaudemans, and P. J. Brussaard, Nucl. Phys. **A549**, 197 (1992).

[57] J. G. L. Booten and A. G. M. van Hees, Nucl. Phys. **A569**, 510 (1994).

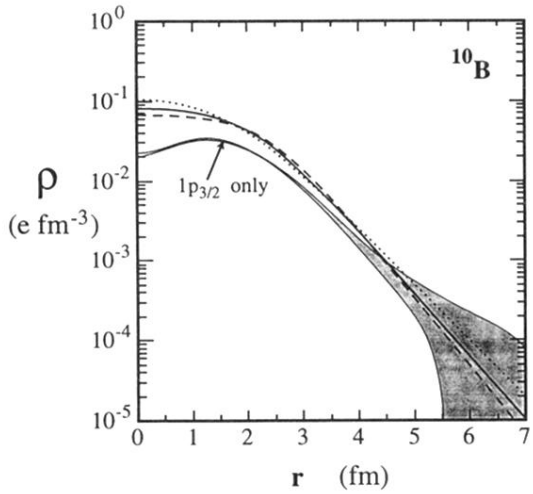

FIG. 5. Ground-state charge densities of ^{10}B, derived from three separate $C2$ models as described in the text. The solid curve is for model (A), dashed curve for model (B), and dotted curve for model (C). The shaded band represents the $1p_{3/2}$ density obtained from a Fourier-Bessel analysis of the $M3$ form factor for the 1.74 MeV transition, normalized to a $1p_{3/2}$-shell occupancy of three protons. The proton size is included in all curves.